Bulk Models of the Sheared Convective Boundary Layer: Evaluation through Large Eddy Simulations

ROBERT CONZEMIUS

School of Meteorology, University of Oklahoma, Norman, Oklahoma, Department of Atmospheric Science, Colorado State University, Fort Collins, Colorado, and Windlogics, Inc., Grand Rapids, Minnesota

EVGENI FEDOROVICH

School of Meteorology, University of Oklahoma, Norman, Oklahoma

(Manuscript received 3 January 2006, in final form 10 July 2006)

ABSTRACT

A set of first-order model (FOM) equations, describing the sheared convective boundary layer (CBL) evolution, is derived. The model output is compared with predictions of the zero-order bulk model (ZOM) for the same CBL type. Large eddy simulation (LES) data are employed to test both models. The results show an advantage of the FOM over the ZOM in the prediction of entrainment, but in many CBL cases, the predictions by the two models are fairly close. Despite its relative simplicity, the ZOM is able to quantify the effects of shear production and dissipation in an integral sense—as long as the constants describing the integral dissipation of shear- and buoyancy-produced turbulence kinetic energy (TKE) are prescribed appropriately and the shear is weak enough that the denominator of the ZOM entrainment equation does not approach zero, causing a numerical instability in the solutions. Overall, the FOM better predicts the entrainment rate due to its ability to avoid this instability. Also, the FOM in a more physically consistent manner reproduces the sheared CBL entrainment zone, whose depth is controlled by a balance among shear generation, buoyancy consumption, and dissipation of TKE. Such balance is manifested by nearly constant values of Richardson numbers observed in the entrainment zone of simulated sheared CBLs. Conducted model tests support the conclusion that the surface shear generation of TKE and its corresponding dissipation, as well as the nonstationary terms, can be omitted from the integral TKE balance equation.

1. Introduction

Since Ball (1960) and Lilly (1968) suggested a bulk model framework describing the evolution of the atmospheric convective boundary layer (CBL), the bulk model approach (Fedorovich 1995, 1998) has been widely used to predict the CBL entrainment rate. This approach has been employed to predict the convective mixed-layer depth for air quality applications (Batchvarova and Gryning 1991; García et al. 2002) and to parameterize boundary layer processes in general circulation models (Haltiner and Williams 1980). Bulk models are also useful for developing a conceptual understanding of processes that are essential to the evolution of the CBL.

The bulk approach generally assumes a horizontally quasi-homogeneous CBL in which horizontal averages can be substituted for ensemble means. Equations describing the CBL evolution are derived by vertically integrating the horizontally averaged variables through the depth of the CBL. The vertical integration is made tractable by employing a schematic representation of the CBL vertical structure, explained in section 2. Such a simplified representation is justified as long as it captures the essential features of the CBL. To obtain a set of equations that expresses the evolution of CBL bulk parameters in the most straightforward manner, Ball (1960) and Lilly (1968) employed a zero-order representation of the CBL structure (see Fig. 1) in which the CBL is represented by a single layer of height-constant buoyancy. Betts (1973), Carson (1973), Stull (1973), and Tennekes (1973) also employed this zero-order approach. The effects of wind shear were excluded in the original versions of the zero-order model (ZOM). Ana-

Corresponding author address: Robert Conzemius, Windlogics, Inc., 201 NW 4th St., Grand Rapids, MN 55744.
E-mail: robert.conzemius@att.net

DOI: 10.1175/JAS3870.1

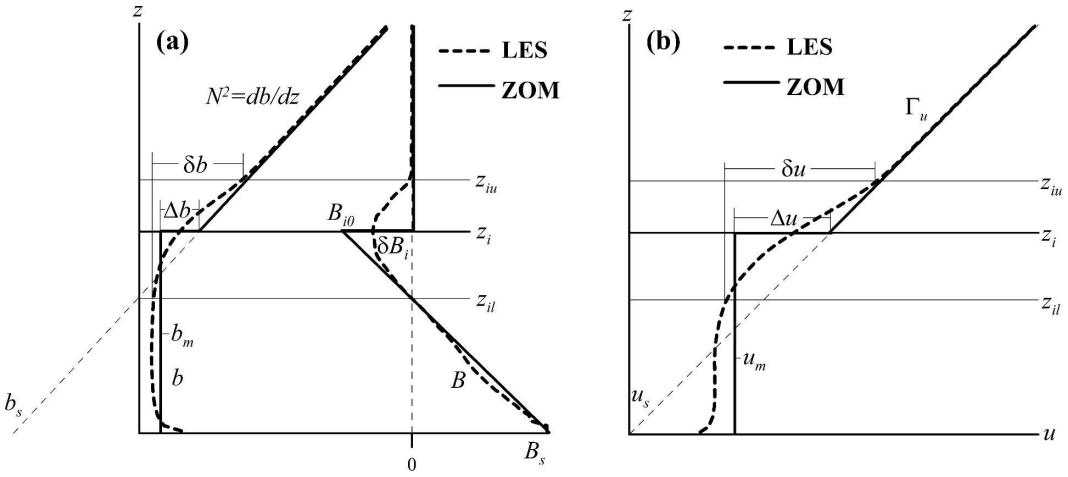

FIG. 1. Profiles of (a) buoyancy b and buoyancy flux B, and (b) the x component of momentum u in the horizontally (quasi) homogeneous CBL. Heavy dashed lines indicate atmospheric (simulated with LES) horizontally averaged profiles, and heavy solid lines indicate their ZOM representation. Lighter solid lines are the lower (z_{il}) and upper (z_{iu}) limits of the entrainment zone, and z_i is the height of the CBL top defined by the minimum of B. The diagonal dashed line in (a) shows the background atmospheric profile of buoyancy $b_s + N^2 z$, where N is the Brunt–Väisälä frequency and b_s is the surface value of background buoyancy; in (b), it shows the profile of geostrophic wind $u_s + \Gamma_u z$, where u_s is the surface value of the geostrophic wind and Γ_u is the x component of the geostrophic shear. For any variable ϕ, $\delta\phi$ is the change of ϕ across the entrainment zone, and $\Delta\phi$ is the ZOM jump of ϕ. The variable B_{i0} represents the ZOM value of the entrainment zone buoyancy flux minimum, B_s is the surface value of the buoyancy flux, and b_m and u_m are the mixed-layer values of buoyancy and x-component velocity, respectively.

lytical ZOM solutions may be obtained for the shear-free CBL after some additional assumptions are made (Zilitinkevich 1991; Fedorovich et al. 2004a). However, most CBLs in nature are not entirely shear free, so Stull (1976a,b,c), Zeman and Tennekes (1977), Tennekes and Driedonks (1981), Driedonks (1982), Boers et al. (1984), Batchvarova and Gryning (1991, 1994), Fedorovich (1995), and Pino et al. (2003) suggested ways to extend the ZOM approach to include the effects of wind shears.

If the CBL structure adopted in the model is oversimplified, processes vital to the CBL evolution may not be sufficiently represented. With this in mind, Betts (1974) proposed the first-order model (FOM) of the shear-free CBL (see Fig. 2). Mahrt and Lenschow (1976, hereafter ML76) extended the FOM to describe height-constant velocity in the CBL mixed layer and linearly changing velocity in the entrainment zone. As such, FOM is the lowest-order model capable of resolving the buoyancy and velocity profiles in the entrainment zone. Higher-order bulk models of entrainment proposed by Deardorff (1979) and Fedorovich and Mironov (1995) have been limited exclusively to the shear-free CBL.

Large eddy simulation (LES) has played a significant role in the studies of sheared CBLs. From this point forward, in order to distinguish between the concepts of simulation and modeling, we will occasionally refer to large eddy–simulated CBLs as simulated CBLs and to the CBLs represented by ZOM and FOM as modeled CBLs. The LES studies of Sorbjan (1996a,b), Lewellen and Lewellen (1998), Sullivan et al. (1998), Van Zanten et al. (1999), and Otte and Wyngaard (2001) have all demonstrated the importance of the inversion-layer structure for the dynamics of the CBL. Otte and Wyngaard (2001) indicated that the stable interfacial (entrainment) layer atop a sheared CBL, behaves similarly to the stable nocturnal boundary layer, with the flux Richardson (Ri) number Ri_f in the layer maintaining a critical value of about 0.3. The dependence of sheared entrainment on the entrainment zone Richardson number, predicted by ML76 and confirmed by Kim et al. (2003), Sorbjan (2004), and Kim et al. (2006, hereafter KPPV) suggests that one needs, as a minimum, FOM representation of the CBL in order to adequately capture the entrainment process in sheared CBLs. The interfacial-layer thickness, in this case, becomes a regulating factor for the ratio of integral shear production of turbulence and integral buoyancy destruction of turbulence (ML76).

The present study is a continuation of the work presented in Conzemius and Fedorovich (2006a, hereafter CFI) and Conzemius and Fedorovich (2006b, hereafter CFII). The results of the LES studies in CFI provide

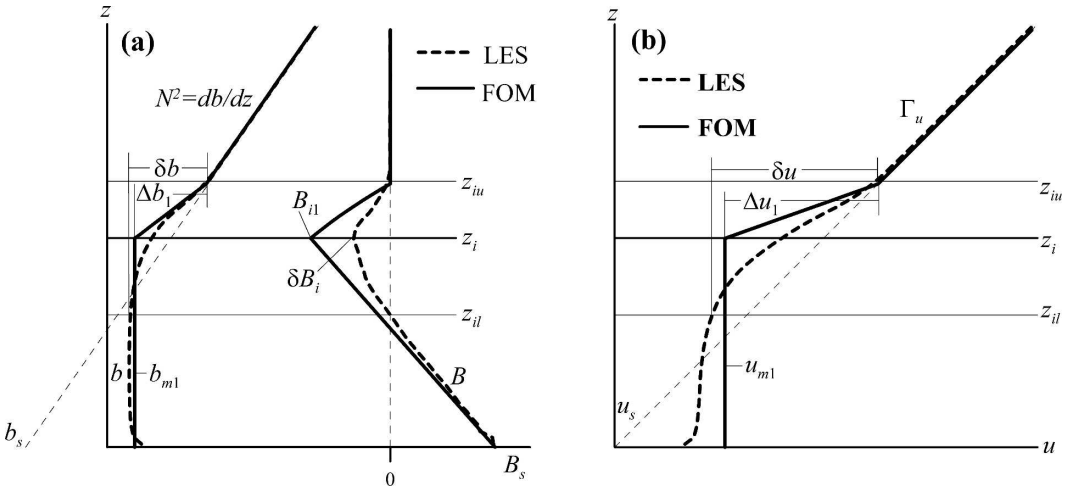

FIG. 2. Profiles of (a) buoyancy and buoyancy flux and (b) velocity in the FOM of the horizontally (quasi) homogeneous CBL. Heavy dashed lines indicate atmospheric (simulated with LES) horizontally averaged profiles, and heavy solid lines indicate their representation in the FOM. Lighter solid lines are the lower (z_{il}) and upper (z_{iu}) limits of the entrainment zone and the height of the CBL top (z_i). Variables have the same meaning as in Fig. 1, but the subscript "1" is added to denote that it is a FOM variable. For any variableϕ, $\Delta\phi_1$ refers to the ϕ change across the CBL top in the FOM.

support for the aforementioned behavior of the entrainment zone Richardson number, yet tests of previously proposed ZOM- and FOM-based entrainment parameterizations against the LES data (CFII) revealed no substantial differences between the overall ability of the ZOM and FOM to predict the entrainment in sheared CBLs. One issue complicating the above tests was that the FOM-based entrainment equations of ML76 and KPPV omitted some features of the CBL structure as represented by the FOM (CFII). While previously derived FOM equations may work very well for a particular subset of CBL types (see, in particular, KPPV), CFI have considered a broader range of atmospheric background conditions, and it is our wish to utilize those results in new FOM-based entrainment equations for sheared CBLs. Two important findings of CFI are the following:

1) The entrainment zone of sheared CBLs develops a balance between shear production and buoyancy destruction of turbulent kinetic energy (TKE), so that entrainment zone Ri numbers attain nearly constant values as shear becomes important to the CBL evolution.
2) The surface shear production of TKE is relatively unimportant for the TKE balance within the context of the entrainment problem.

The current study seeks to provide answers to the following questions regarding the application of the bulk model equations to sheared CBLs:

1) Is it necessary to use the FOM to adequately describe the evolution of the sheared CBL, or is the ZOM CBL structure representation sufficient for this purpose? In other words, what is the importance of the finiteness of the interfacial-layer thickness for the modeling of entrainment?
2) What is the sensitivity of the FOM predictions of sheared CBL evolution to the modeled entrainment zone Ri?
3) Is surface layer shear-produced turbulence unimportant for the entrainment as reproduced by the FOM? That is, can the sheared CBL evolution be successfully modeled if surface shear-produced TKE is omitted from the TKE balance?

The remaining portions of the text are organized as follows: a derivation of the FOM equations for the horizontally homogeneous sheared CBL is presented in section 2; section 3 describes the procedure by which these FOM equations are evaluated against LES data; section 4 contains the results of model evaluations; and section 5 reviews and summarizes the overall findings of the study.

2. Derivation of FOM equations

a. Governing equations for the horizontally homogeneous CBL flow

Within the ZOM and FOM frameworks (see schematics in Figs. 1 and 2), the entrainment equations are

derived for a horizontally homogeneous, temporally evolving CBL flow, in which the horizontally averaged flow statistics are assumed to converge to corresponding ensemble means. Under these assumptions, the Reynolds-averaged Navier–Stokes (RANS) equations for horizontally homogeneous (in a statistical sense), nonstationary CBL flow reduce to (see CFII)

$$\frac{\partial b}{\partial t} = -\frac{\partial B}{\partial z}, \tag{1}$$

$$\frac{\partial u}{\partial t} = \frac{\partial \tau_x}{\partial z} + f(v - v_g), \tag{2}$$

$$\frac{\partial v}{\partial t} = \frac{\partial \tau_y}{\partial z} - f(u - u_g), \tag{3}$$

$$\frac{\partial e}{\partial t} = \tau_x \frac{\partial u}{\partial z} + \tau_y \frac{\partial v}{\partial z} + B - \frac{\partial \Phi}{\partial z} - \varepsilon, \tag{4}$$

where the mean buoyancy is approximated as $b = g(\theta - \theta_0)/\theta_0$, g is the gravitational acceleration, θ is potential temperature (to be inclusive of water vapor, θ could also represent virtual potential temperature), θ_0 is its reference value, $B = (g/\theta_0)\, Q_s$ is the vertical buoyancy flux (Q_s is the kinematic heat flux), the mean velocity components are u and v, the corresponding components of vertical turbulent kinematic fluxes are $\tau_x = -\overline{w'u'}$ and $\tau_y = -\overline{w'v'}$, u_g and v_g are the geostrophic wind components, f is the Coriolis parameter, e is the TKE per unit mass, Φ is the TKE vertical flux, and ε is the TKE dissipation rate.

Sorbjan (2004) considered the effect of horizontal temperature advection on the buoyancy (potential temperature) balance in (2) that can modify the evolution of baroclinic CBLs. Although we have derived and tested versions of our FOM that include the effects of temperature advection, the LES data in CFI were generated for barotropic and equivalent barotropic conditions when the aforementioned effects were insignificant, so those effects are excluded in the present study.

b. Integral buoyancy, momentum, and TKE budgets

Five equations are required in the FOM (see Fig. 2) to describe the dependent variables Δb, Δu, Δv, z_i, and Δz in terms of the independent variables t, B_s, Γ_u, Γ_v, and N. To obtain the first four equations, we integrate (1)–(4) over the depth of the CBL and come up with CBL integral buoyancy, momentum, and TKE budgets, respectively (see the appendix for details):

$$\frac{d}{dt}\left[\frac{N^2(z_i + \Delta z)^2}{2} - \Delta b_1\left(z_i + \frac{\Delta z}{2}\right)\right] = B_s, \tag{5}$$

$$\frac{d}{dt}\left[\frac{\Gamma_u(z_i + \Delta z)^2}{2} - \Delta u_1\left(z_i + \frac{\Delta z}{2}\right)\right] = -\tau_{xs} + f\left[\frac{\Gamma_v(z_i + \Delta z)^2}{2} - \Delta v_1\left(z_i + \frac{\Delta z}{2}\right)\right], \tag{6}$$

$$\frac{d}{dt}\left[\frac{\Gamma_v(z_i + \Delta z)^2}{2} - \Delta v_1\left(z_i + \frac{\Delta z}{2}\right)\right] = -\tau_{ys} - f\left[\frac{\Gamma_u(z_i + \Delta z)^2}{2} - \Delta u_1\left(z_i + \frac{\Delta z}{2}\right)\right], \tag{7}$$

$$\int_0^{z_i+\Delta z} \frac{\partial e}{\partial t}\, dz = \int_0^{z_i+\Delta z} S\, dz + \int_0^{z_i+\Delta z} B\, dz - \int_0^{z_i+\Delta z} \varepsilon\, dz, \tag{8}$$

where

$$\begin{aligned}\int_0^{z_i+\Delta z} S\, dz = {} & [u_s + \Gamma_u(z_i + \Delta z) - \Delta u_1]\tau_{xs} \\ & + [v_s + \Gamma_v(z_i + \Delta z) - \Delta v_1]\tau_{ys} \\ & + \frac{1}{2}(\Delta u_1^2 + \Delta v_1^2)\frac{d}{dt}\left(z_i + \frac{2}{3}\Delta z\right) \\ & + \frac{\Delta z}{12}\frac{d}{dt}(\Delta u_1^2 + \Delta v_1^2) \\ & - \frac{\Delta z}{2}(\Gamma_u \Delta u_1 + \Gamma_v \Delta v_1)\frac{d}{dt}(z_i + \Delta z) \\ & + f\frac{\Delta z^2}{6}(\Gamma_v \Delta u_1 - \Gamma_u \Delta v_1),\end{aligned} \tag{9}$$

and

$$\begin{aligned}\int_0^{z_i+\Delta z} B\, dz = {} & \frac{1}{2} B_s(z_i + \Delta z) - \frac{1}{2} z_i \Delta b_1 \frac{dz_i}{dt} \\ & + \frac{1}{4}\left(z_i + \frac{\Delta z}{3}\right)\left(\Delta z \frac{d\Delta b_1}{dt} - \Delta b_1 \frac{d\Delta z}{dt}\right).\end{aligned} \tag{10}$$

c. Equation for entrainment zone thickness

An equation for Δz is needed to close the set. Based on the results of ML76, Otte and Wyngaard (2001), and CFI, we have chosen to determine Δz based on the constraint of a constant Ri in the entrainment zone. We define a FOM-specific bulk gradient Richardson number

$$\mathrm{Ri}_1 = \frac{\Delta z \Delta b_1}{\Delta u_1^2 + \Delta v_1^2}, \tag{11}$$

and set it to a constant critical value of $\mathrm{Ri}_1 = 0.15$ (see discussion in section 4 on the model sensitivity to this parameter). The adopted formulation for Δz gives the proposed bulk model a special property: the entrainment layer of finite thickness Δz arises only due to the effects of the mean shear across the CBL top. When this shear is zero, Δz collapses to zero, and the whole bulk model reduces from first order to zero order.

The constraint in (11) is a somewhat unsettled subject. Indeed, local Richardson numbers are variable in the entrainment zones of sheared CBLs. Our tests of a parameterization for the entrainment zone buoyancy flux based on such Ri behavior (Sorbjan 2004) showed good agreement with LES data (CFII). Similarly, the fact that the entrainment zone thickness is finite also under shear-free conditions (Sullivan et al. 1998; Lilly 2002a; Fedorovich et al. 2004a) suggests that (11) could be altered in order to account for the nonzero entrainment zone depth in the shear-free CBL, for instance, by incorporating the Deardorff (1970) convective velocity scale $w_* = (B_s z_i)^{1/3}$ in the denominator of (11).

After strongly considering alternative formulations for the entrainment zone Richardson number, we have decided to retain the formulation as shown in (11). The reasons for our decision are the following:

1) Incorporating w_* does not solve the problem of model predictions of entrainment zone thickness for shear-free cases; see our analysis in section 4.
2) Shear may exist locally at the entrainment interface of shear-free CBL, but this shear disappears when ensemble- or horizontal-averaging techniques are applied. The fundamental equations of the proposed FOM should reflect this feature.
3) We wish to promote the concept of entrainment-layer thickness responding to the mean shear across the CBL top. Besides being illustrative and physically meaningful, this concept provides a convenient framework for testing hypotheses about the dynamics of the sheared CBL entrainment.

Our understanding of the entrainment zone thickness in the shear-free limit is consistent with (but not entirely based upon) the work of Lilly (2002a,b), who noticed that the entrainment interface remains sharp locally, and its finite thickness seen in horizontally averaged profiles is just the result of horizontal averaging. Certainly, lidar data (Kiemle et al. 1995) show that, even locally, the interface is not always sharp, and it can be argued (Stull 1988) that shear contributes locally to the structure of the entrainment zone in shear-free CBLs.

ML76 have discussed aircraft measurements of the sheared interfacial layer atop the atmospheric CBL, and these measurements indicated that the entrainment zone Ri maintained a nearly constant, critical value. Otte and Wyngaard (2001) have presented simulation data, which also suggest that the interfacial-layer Ri behaves in this manner. Our LES results presented in CFI show that the flux Richardson number, Ri_f (see section 4c), in the entrainment zone approaches an approximately constant value in nearly all the simulated CBL cases in which shear was a contributor to entrainment. However, setting a criterion for Ri_f in the entrainment zone would lead to a rather cumbersome expression involving both (9) and (10), so we have chosen to implement the bulk Ri approach in (11). Provided the shear is sufficiently strong, the gradient Richardson number, Ri_g (see section 4c), is approximately constant in the entrainment zone of sheared CBLs (CFI). ML76 have also pointed to Ri_1, Eq. (11), as a reasonable substitute for Ri_f. One can thus expect that a bulk version of Ri in the entrainment zone will be a good approximation for Ri_f.

In essence, the CBL is represented as a single-layer entity in the shear-free case. When shear is present, it acquires a two-layer structure, composed of a layer of height-constant buoyancy and velocity, which is similar to the shear-free CBL, topped by a shear-driven layer whose turbulence is maintained by a balance among shear generation of TKE, buoyancy consumption of TKE, and dissipation. This structure matches the two-layer CBL concept proposed by Lewellen and Lewellen (2000), who suggested that the sheared CBL can be considered as two separate turbulent layers: a buoyancy-driven mixed layer topped by a shear-driven layer.

d. Scalings

There are still several unknown terms in the system of model equations. The first of these are the surface velocity fluxes $-\tau_{xs}$ and $-\tau_{ys}$. We parameterize these fluxes by employing the following surface drag relations (Garratt 1992):

$$\tau_{xs} = C_D u_{m1}(u_{m1}^2 + v_{m1}^2)^{1/2}, \tag{12}$$

$$\tau_{ys} = C_D v_{m1}(u_{m1}^2 + v_{m1}^2)^{1/2}. \tag{13}$$

From the LES data (CFI), a value of $C_D = 0.002$ was estimated.

Next, scaling considerations need to be applied to the integral dissipation. Based on the LES estimates, we may assume that the dissipation of TKE is proportional to its production and that the dissipation rate is a linear combination of contributions from all the production

mechanisms. This assumption is made explicitly in KPPV, and it is also made implicitly in several previously suggested versions of ZOM by the use of scaling constants associated with the production terms in the ZOM TKE balance equation (Tennekes and Driedonks 1981; Driedonks 1982; Boers et al. 1984; Pino et al. 2003). With these assumptions, the integral of dissipation takes the following form:

$$\int_0^{z_i+\Delta z} \varepsilon \, dz = \int_0^{z_i+\Delta z} \varepsilon_{sS} \, dz + \int_0^{z_i+\Delta z} \varepsilon_{eS} \, dz + \int_0^{z_i+\Delta z} \varepsilon_B \, dz. \tag{14}$$

Hence, the integral dissipation rate includes the dissipation of the TKE produced by the surface shear, ε_{sS}, and entrainment zone shear, ε_{eS}, and the dissipation of the TKE produced by the buoyancy flux, ε_B. For the dissipation of the buoyantly produced TKE, we employ the same scaling hypothesis that is used in the ZOM (Zilitinkevich 1991):

$$\int_0^{z_i+\Delta z} \varepsilon_B \, dz = C_{\varepsilon B} w_*^3, \tag{15}$$

with $C_{\varepsilon B} = 0.4$. Since dissipation occurs throughout the depth of the turbulent layer, which extends to $z = z_i + \Delta z$, the scaling (15) may appear to be incomplete, but there are two reasons to use it in this particular form. First, in the proposed bulk model, the interfacial layer of finite thickness Δz develops only in response to mean shear at the CBL top, and it is assumed that the production and dissipation of buoyancy-generated TKE is not affected by shear. To be consistent with these assumptions, and given the fact that the proposed model reverts to the ZOM in the shear-free case, we keep the scaling associated with buoyancy-generated TKE the same as in the ZOM. Furthermore, the LES data (Fedorovich et al. 2004a; CFI) show that the scaling (15) is rather robust. Attempts to include Δz in the defining expression for w_* caused the model equations to become too dissipative and, as result, forced the modeled CBL to grow much more slowly than the simulated CBL.

For the dissipation of entrainment zone shear-generated TKE, ε_{eS}, a number of scaling hypotheses were considered. It turned out most tenable to assume, as in previous studies (Tennekes and Driedonks 1981; Driedonks 1982; Boers et al. 1984; Pino et al. 2003), that a nearly constant fraction of the shear-produced TKE is available for entrainment with the rest being dissipated. That is, the dissipation of shear-generated TKE scales according to its production. Other considered scaling approaches resulted in a decoupling of the dissipation of shear-generated TKE from its production, causing problematic mathematical behavior of the system of equations. Our LES results (CFI) indicate the fraction of entrainment zone shear-produced TKE available for entrainment to be $C_P = 0.4$, so the effects of corresponding dissipation are parameterized by multiplying the last four lines of (9) by $C_P = 0.4$.

The LES of sheared CBLs (CFI) have shown that the surface layer shear does not directly contribute to the TKE available for entrainment because the shear generation of TKE in the surface layer is essentially balanced by dissipation. This finding is in agreement with the analyses of atmospheric datasets (Lenschow 1970, 1974) for CBL cases with surface layer shear and supports a related hypothesis adopted in the FOM of ML76. On these grounds, we remove the surface-shear generation of TKE from Eq. (9) since the corresponding term does not seem to be of direct importance for the entrainment prediction. However, because the surface layer shear influences the mixed-layer velocity field and thus indirectly affects the entrainment zone shear (ML76; CFI), it is retained in the momentum equations. It is through the momentum balance Eqs. (6) and (7) that the effects of surface layer shear are felt on entrainment.

The choice of scaling for the left-hand side of (8) is a bit more troublesome. Data from previous LES studies indicate considerable uncertainty regarding this so-called TKE spinup term (Zilitinkevich 1991). Fedorovich et al. (2004a) have shown that, in the shear-free CBL context, this term can be omitted from the ZOM TKE balance even at early stages of the CBL development, provided dissipation is scaled appropriately. Likewise, our own attempts to include the nonstationary term in the TKE balance equation have shown that it adversely affects the ability of the bulk model–based equations to predict the CBL growth. A complete investigation into this matter deserves the full treatment through a separate study, but our present understanding is that neither the dissipation nor the spinup is perfectly described using the traditional scaling methodology. Rather, the two processes appear to produce a combined effect on the availability of TKE for entrainment that is well quantified by employing the dissipation scaling alone. Fedorovich et al. (2004b) presented some preliminary analyses addressing the nonstationarity of TKE budget of shear-free CBLs.

e. Final set of FOM equations

With the above-discussed modifications to the set of equations, we come to the final set of FOM equations for the sheared CBL to be evaluated in the present study:

$$\frac{d}{dt}\left[\frac{N^2(z_i+\Delta z)^2}{2}-\Delta b_1\left(z_i+\frac{\Delta z}{2}\right)\right]=B_s, \tag{16}$$

$$\frac{d}{dt}\left[\frac{\Gamma_u(z_i+\Delta z)^2}{2}-\Delta u_1\left(z_i+\frac{\Delta z}{2}\right)\right]=-C_D u_{m1}(u_{m1}^2+v_{m1}^2)^{1/2}+f\left[\frac{\Gamma_v(z_i+\Delta z)^2}{2}-\Delta v_1\left(z_i+\frac{\Delta z}{2}\right)\right], \tag{17}$$

$$\frac{d}{dt}\left[\frac{\Gamma_v(z_i+\Delta z)^2}{2}-\Delta v_1\left(z_i+\frac{\Delta z}{2}\right)\right]=-C_D v_{m1}(u_{m1}^2+v_{m1}^2)^{1/2}-f\left[\frac{\Gamma_u(z_i+\Delta z)^2}{2}-\Delta u_1\left(z_i+\frac{\Delta z}{2}\right)\right], \tag{18}$$

$$C_P\left[\begin{array}{l}\frac{1}{2}(\Delta u_1^2+\Delta v_1^2)\frac{d}{dt}\left(z_i+\frac{2}{3}\Delta z\right)+\frac{\Delta z}{12}\frac{d}{dt}(\Delta u_1^2+\Delta v_1^2)\\ -\frac{\Delta z}{2}(\Gamma_u\Delta u_1+\Gamma_v\Delta v_1)\frac{d}{dt}(z_i+\Delta z)+f\frac{\Delta z^2}{6}(\Gamma_v\Delta u_1-\Gamma_u\Delta v_1)\end{array}\right]+\frac{1}{2}B_s(z_i+\Delta z)-\frac{1}{2}z_i\Delta b_1\frac{dz_i}{dt}$$
$$+\frac{1}{4}\left(z_i+\frac{\Delta z}{3}\right)\left(\Delta z\frac{d\Delta b_1}{dt}-\Delta b_1\frac{d\Delta z}{dt}\right)-C_{\varepsilon B}B_s z_i=0, \tag{19}$$

$$\mathrm{Ri}_1=\frac{\Delta z\Delta b_1}{\Delta u_1^2+\Delta v_1^2}=0.15, \tag{20}$$

with $u_{m1}=u_s+\Gamma_u(z_i+\Delta z)-\Delta u_1$ and $v_{m1}=v_s+\Gamma_v(z_i+\Delta z)-\Delta v_1$. Equations (16)–(20) are a set of five equations for the five unknowns: Δb_1, Δu_1, Δv_1, z_i, and Δz.

f. Corresponding set of ZOM equations

In the ZOM equations for the entraining sheared CBL (Fedorovich 1995; CFII), the same assumptions regarding the TKE source and sink terms may be applied. The dissipation terms are scaled in the same manner as described in section 2c, the nonstationary terms are omitted, and surface shear production of TKE, presumably balanced by dissipation, is removed from the TKE equation. The momentum equations include the drag coefficient parameterizations for the momentum fluxes at the surface analogous to (12) and (13). The following ZOM equations for four unknowns Δb, Δu, Δv, and z_i are the following:

$$\frac{d}{dt}\left(\frac{N^2z_i^2}{2}-\Delta b z_i\right)=B_s, \tag{21}$$

$$\frac{d}{dt}\left(\frac{\Gamma_u z_i^2}{2}-\Delta u z_i\right)=-C_D u_m(u_m^2+v_m^2)^{1/2}+f\left(\frac{\Gamma_v z_i^2}{2}-\Delta v z_i\right), \tag{22}$$

$$\frac{d}{dt}\left(\frac{\Gamma_v z_i^2}{2}-\Delta v z_i\right)=-C_D v_m(u_m^2+v_m^2)^{1/2}-f\left(\frac{\Gamma_u z_i^2}{2}-\Delta u z_i\right), \tag{23}$$

$$\frac{1}{2}C_P(\Delta u^2+\Delta v^2)\frac{dz_i}{dt}+\frac{1}{2}B_s z_i-\frac{1}{2}z_i\Delta b\frac{dz_i}{dt}-C_{\varepsilon B}B_s z_i=0, \tag{24}$$

with $u_m=u_s+\Gamma_u z_i-\Delta u$ and $v_m=v_s+\Gamma_v z_i-\Delta v$. These ZOM equations will be evaluated in section 4 along with the FOM equations (16)–(20).

3. Model evaluation: Procedures and data

a. LES data

The derived bulk model equations were integrated and compared to the output of 24 LES runs for different sheared CBL types described in CFI: cases with no shear and no background flow (NS); cases in which the geostrophic wind started at 0 m s^{-1} at the surface and increased to 20 m s^{-1} at the top of the simulation domain (GS); and cases with height-constant geostrophic wind of 20 m s^{-1} throughout the depth of the domain (GC). The sheared CBL cases were designed to distinguish between the effects of surface layer shear (i.e., GC) and entrainment zone, or elevated, shear (i.e., GS), see CFI.

b. Integration procedure

The FOM-based equations (16)–(20) and the ZOM-based equations (21)–(24) were integrated using the Newton–Ralphson method (Press et al. 1992). The numerical runs for both sets of equations were initialized with the CBL depth z_i, mixed-layer buoyancy (b_{m1} or b_m), and velocity components (u_{m1} and v_{m1}, or u_m and v_m) retrieved from LES output data at some time t_0

early in the simulation. The procedure for obtaining these parameters from the LES data is defined in CFII and schematized graphically in Figs. 1 and 2. To reduce the scatter in the estimated CBL parameters due to finite sampling size in the horizontal averaging process, the parameters were subjected to a prior least squares fit with fitting functions chosen by visual inspection of the simulation data. These functions are listed in Table 1. The fit was started when an entraining, turbulent CBL was first detected in the simulation and ended at the termination of the simulation. The start times are shown in Table 1. The LES data at times prior to the development of a turbulent CBL were excluded from the presented analyses.

The fitted mixed-layer variables were then employed, along with the atmospheric background profiles of velocity and buoyancy, to compute initial Δu_1, Δv_1, Δb_1, and Δz in the FOM, using $\mathrm{Ri}_1 = 0.15$ as a constraint [see Eq. (11)]. We have chosen to use this method for the determination of Δu_1, Δv_1, Δb_1, and Δz because obtaining them directly from the LES data leads to considerable scatter in their estimates (due to scatter in z_i). To obtain the initial buoyancy and velocity jumps at the CBL top in the ZOM, the relations $\Delta u = u_s + \Gamma_u z_i - u_m$ and $\Delta v = v_s + \Gamma_v z_i - v_m$ were used.

The bulk model equations are susceptible to predicting unrealistic entrainment rates if the assumptions regarding the dissipation and nonstationary terms are inappropriately formulated (see discussion in CFII). This susceptibility can be illustrated for the ZOM by solving (24) for dz_i/dt:

$$\frac{dz_i}{dt} = B_s z_i \frac{C_1}{[\Delta b z_i - C_P(\Delta u^2 + \Delta v^2)]}, \qquad (25)$$

with $C_1 = (1 - 2C_{\varepsilon B})$. Likewise, the FOM equation, (19), provides, for dz_i/dt, the expression of the form

$$\frac{dz_i}{dt} \propto \{\Delta b_1 z_i - C_P[(\Delta u_1^2 + \Delta v_1^2) - \Delta z(\Gamma_u \Delta u_1 + \Gamma_v \Delta v_1)]\}^{-1}. \qquad (26)$$

If the effects of shear are sufficiently strong, the denominators of both (25) and (26) may approach zero, causing the equations to predict nearly infinite entrainment rates. If the shear term increases further, (25) and (26) will predict negative entrainment rates. It is relatively easy to see from (26) that the FOM is less susceptible to such instabilities because the term involving Δz offsets the term involving the squares of the entrainment zone velocity jumps Δu_1 and Δv_1.

Because the equations are most susceptible to these problems at small t when dz_i/dt is large anyway, and in order to investigate whether the equations behave in a more realistic manner at larger t, we opted to reinitialize the equations if the predicted entrainment rate dz_i/dt or the buoyancy jump (Δb or Δb_1) became less than zero. If reinitialization became necessary, the time t_0 was incremented 100 s beyond the previous initialization time. This reinitialization procedure was repeated until the code was able to integrate the model equations successfully through the end of the simulation period. The model integration was stopped when $z_i > 1000$ m.

TABLE 1. Functions chosen for FOM fits to LES data. Here, 1 is $y = Bt^A$, 2 is $y = A + Bt + Ct^2 + Dt^3$, 3 is $y = Bt^A + C$, and y stands for z_i, u_{m1}, u_m, v_{m1}, v_m, b_{m1}, or b_m.

Q_s (K m s^{-1})	0.03		0.10			
$\partial\theta/\partial z$ (K m^{-1})	0.003		0.003		0.010	
Shear (s^{-1})	0.0125	0	0.0125	0	0.0125	0
Start t_0 (s)	100	3000	100	1000	100	3000
z_i	1	1	1	1	1	1
u_{m1}, u_m	1	2	1	2	1	2
v_{m1}, v_m	2	2	2	2	2	2
b_{m1}, b_m	3	3	3	3	3	3

4. Results of model evaluations

Because of the large number of CBL cases examined, we present here only a representative sample of the model evaluation results in order to describe the overall behavior of the bulk model solutions when compared with LES data. A more complete analysis of the LES results is provided in CFI. The reader is referred to that paper for the details of the findings.

a. Evaluation of FOM predictions

1) PREDICTIONS OF CBL EVOLUTION

Overall, the FOM system of CBL budget equations is able to reproduce the evolution of the CBL depth z_i reasonably well for nearly all of the investigated CBL cases (see Fig. 3). It is also able to adequately reproduce the qualitative differences in the growth rate among the simulated NS-, GS-, and GC-case CBLs described in CFI. In the cases with $\partial\theta/\partial z = 0.010$ K m^{-1} and $Q_s = 0.10$ K m s^{-1} (Fig. 3b), the GC-case CBL grew the fastest, the NS-case CBL the slowest, and the GS-case CBL was in between. The shear enhancement of entrainment was larger in the GC-case than the GS-case CBL because of the larger entrainment zone shear in the GC case. These differences are captured by the FOM with a fair degree of accuracy.

Due to weaker entrainment zone shear in the GC-case CBL, the behavioral features of the simulated GS-case and GC-case CBLs were essentially the opposite

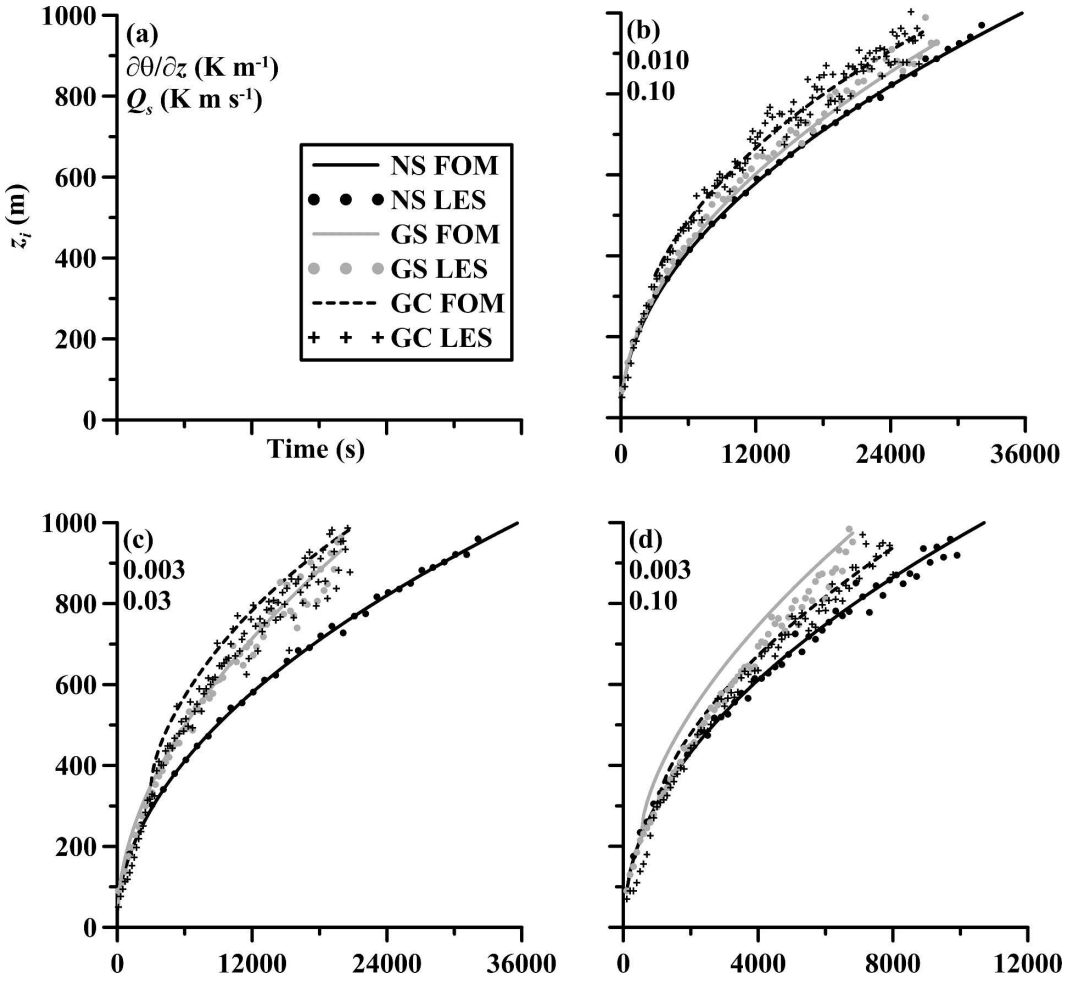

FIG. 3. Comparison of CBL depth z_i vs time predicted by the FOM and by LES for six different CBLs: (a) the legend, (b) $\partial\theta/\partial z = 0.010$ K m^{-1} and $Q_s = 0.1$ K m s^{-1}, (c) $\partial\theta/\partial z = 0.003$ K m^{-1} and $Q_s = 0.03$ K m s^{-1}, and (d) $\partial\theta/\partial z = 0.003$ K m^{-1} and $Q_s = 0.1$ K m s^{-1}. The FOM predictions are denoted by solid black lines for the NS-case CBLs, solid gray lines for the GS-case CBLs, and dashed black lines for the GC-case CBLs. The LES data are indicated by black dots (NS case), gray dots (GS case), and black crosses (GC case).

for the cases with $\partial\theta/\partial z = 0.003$ K m^{-1} and $Q_s = 0.10$ K m s^{-1} (Fig. 3d). The model was still able to account for those differences, although the modeled GS-case CBL growth rate was slightly larger than the simulated growth rate. In this case, CBL growth forced by buoyancy flux from the surface occurs faster than turbulence can mix the momentum in the interior of the CBL and concentrate shear at the CBL top, where the shear generation of TKE can directly influence the entrainment rate. In the FOM, this concentration of the shear in the entrainment zone occurs instantaneously because the velocity in the CBL interior is always perfectly mixed. This result highlights one general shortcoming of mixed-layer models when it comes to predictions of CBL evolution: they do not adequately describe momentum distribution in the CBL interior.

In Fig. 3c, the simulated GS-case and GC-case CBLs grew at nearly equal rates (due to the entrainment zone shear in both cases being nearly equal), and the shear enhancement of entrainment was the strongest of all cases shown. Again, this is a case in which the CBL growth was relatively slow compared to the other cases in which the surface buoyancy flux was stronger or the upper buoyancy stratification weaker. This behavior was also captured by the model, indicating that it is handling the effects of stratification and surface buoyancy flux in a manner consistent with LES predictions of the CBL development. The rate at which velocity and buoyancy become mixed in the CBL interior is comparable to the entrainment rate, allowing mixed-layer models to describe the CBL evolution rather well. It is important to note that the proposed model is able

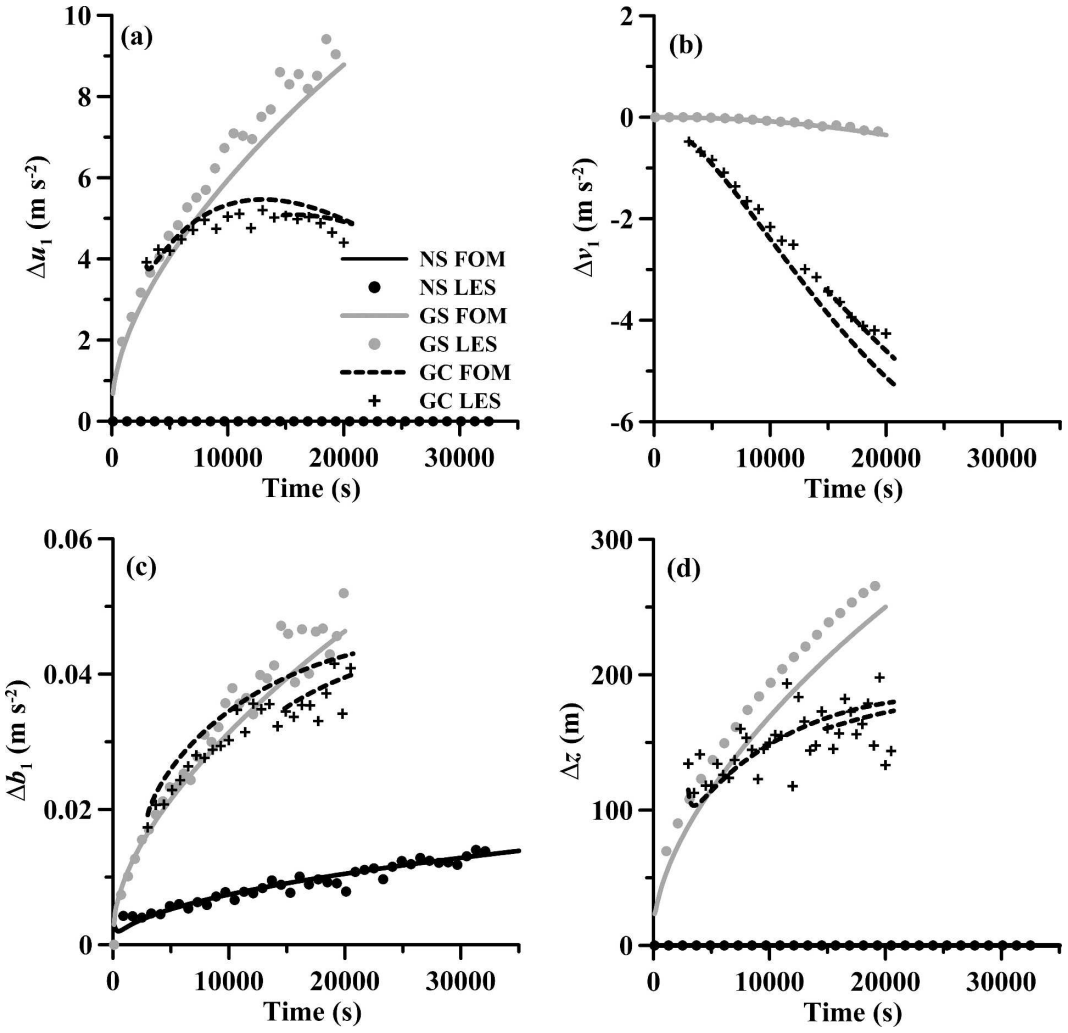

FIG. 4. Predictions of entrainment parameters by the FOM for the CBL cases with $\partial\theta/\partial z = 0.003$ K m^{-1} and $Q_s = 0.03$ K m s^{-1}: (a) jump of the u velocity component, Δu_1; (b) jump of the v velocity component, Δv_1; (c) buoyancy jump Δb_1; and (d) entrainment zone thickness Δz. The FOM predictions are denoted by solid black lines for the NS-case CBLs, solid gray lines for the GS-case CBLs, and dashed black lines for the GC-case CBLs. LES data are indicated by black dots (NS case), gray dots (GS case), and black crosses (GC case). For the GC-case CBL, the second dashed black line in each panel represents an additional FOM run whose initialization time was chosen to correspond with the ZOM.

to capture this behavior without a surface-shear term in the integral TKE equation.

2) OTHER FOM-PREDICTED PARAMETERS OF ENTRAINMENT

The entrainment zone parameters were retrieved from the LES data using the same procedure as was used for the FOM initialization described in section 3b, except that the LES data were used directly, without the least squares fits. The FOM-predicted parameters show reasonably good agreement with the LES-derived parameters (see Fig. 4). The velocity jump Δv_1 in the modeled GC-case CBL is slightly smaller than Δv_1 from the LES. Some of this difference can likely be removed by tuning the drag coefficient C_D to the LES data, but this parameter changes according to the surface roughness anyway, so its tuned value would only be relevant to the particular settings used in LES. The FOM-predicted velocity jump Δu_1 is slightly larger than the LES values, and this is consistent with the larger Δb_1 in the GC-case CBL.

In the GS-case CBL, the entrainment zone parameters Δu_1 and Δz were slightly underpredicted by the FOM-based system of equations, but the parameters Δv_1 and Δb_1 were predicted reasonably well. Overall, it appears that the differences between the NS-, GS-, and GC-case CBLs were predicted relatively well by the proposed bulk model.

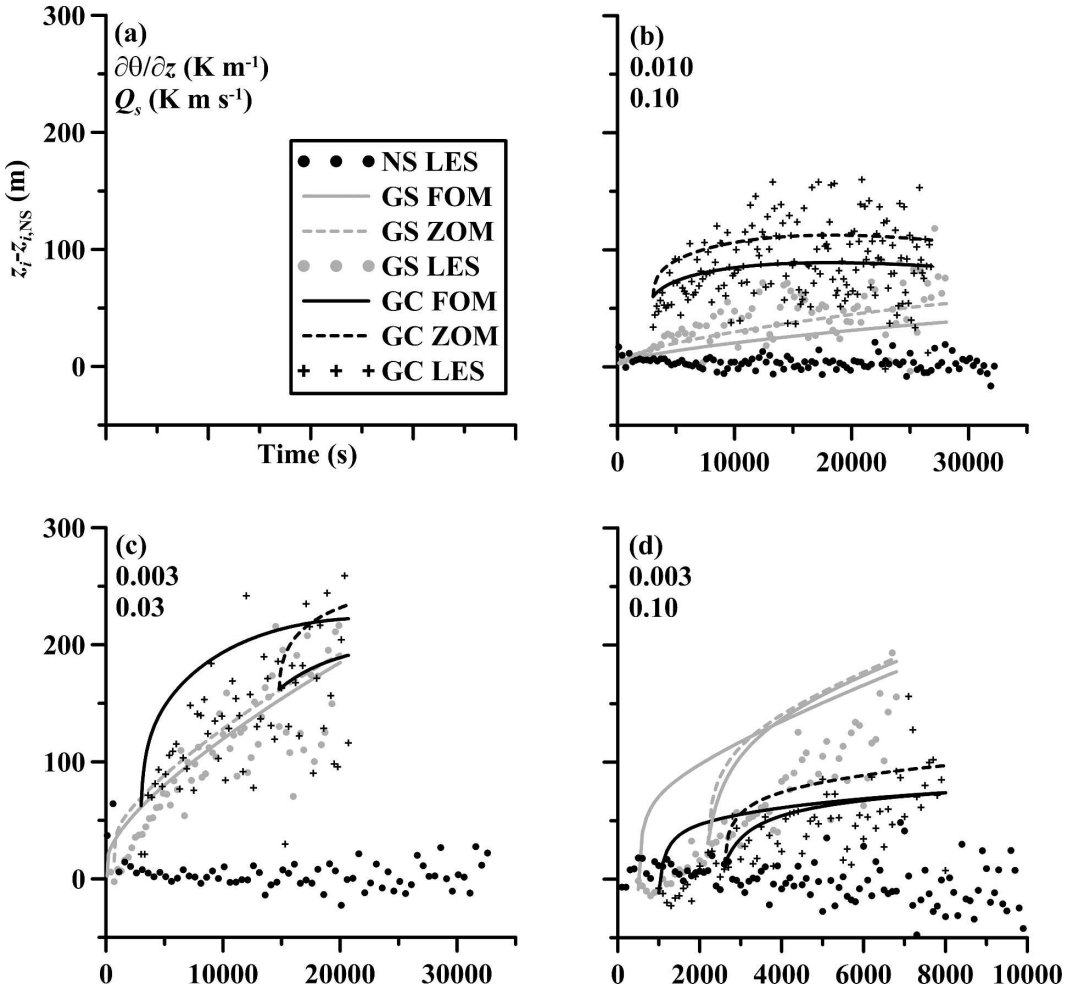

FIG. 5. Comparison of shear enhancement of the CBL growth predicted by the FOM and by LES for the following CBL cases: (a) legend, (b) $\partial\theta/\partial z = 0.010$ K m^{-1} and $Q_s = 0.1$ K m s^{-1}, (c) $\partial\theta/\partial z = 0.003$ K m^{-1} and $Q_s = 0.03$ K m s^{-1}, and (d) $\partial\theta/\partial z = 0.003$ K m^{-1} and $Q_s = 0.1$ K m s^{-1}. The FOM predictions are denoted by solid gray lines for the GS-case CBLs and solid black lines for the GC-case CBLs. The ZOM predictions are indicated by dashed gray lines for the GS-case CBLs and dashed black lines for the GC-case CBLs. The LES data are indicated by black dots (NS case), gray dots (GS case), and black crosses (GC case).

b. Sensitivity to type of bulk model

1) COMPARISON WITH ZOM

The above results do not directly address the impact of the inclusion of a finite entrainment zone thickness on the ability of a bulk model to predict entrainment. In this section, we provide a direct comparison between the FOM and the ZOM, which indicates, in particular, that the ZOM- and FOM-predicted CBL growth rates are not much different from one another. However, the higher instability of the ZOM-derived system of equations discussed in section 3b makes the FOM predictions of CBL evolution generally more reliable than those of the ZOM.

In a majority of cases, the ZOM was generally able to reproduce the sheared CBL growth rates, as well as the differences among the NS-, GS-, and GC-case CBLs. Since the presented FOM reverts to the ZOM for the NS cases, the predictions of the two models are exactly the same in those cases, so the comparison between them is only shown for the sheared CBL cases. Because of the small differences between the FOM- and ZOM-predicted entrainment rates, Fig. 5 shows the shear enhancement of entrainment (sheared CBL minus the corresponding NS-case CBL) in order to elucidate those differences.

In Table 2, we provide a comparison of normalized z_i mean absolute errors for ZOM and FOM. The mean absolute error was calculated as $|z_{i,\mathrm{model}} - z_{i,\mathrm{LES}}|$ and normalized by the CBL depth $z_{i,\mathrm{LES}}$. Both models were

TABLE 2. Mean normalized absolute error of modeled CBL depth z_i.

$\partial\theta/\partial z$ (K m^{-1})	Q_s (K m s^{-1})	Shear	ZOM	FOM
0.003	0.03	GS	0.060	0.055
0.003	0.03	GC	0.062	0.045
0.003	0.10	GS	0.088	0.080
0.003	0.10	GC	0.045	0.027
0.010	0.10	GS	0.021	0.028
0.010	0.10	GC	0.041	0.031

initialized at the same time from the same starting conditions. Only time periods over which both models were stable were included in the analysis. Since the ZOM was sometimes unstable at early stages of the integration, this often required a restart of the FOM at a later time when the ZOM became stable. In those cases, a second line showing FOM-predicted z_i is shown in Figs. 5c,d.

In all cases but one, the FOM was able to more closely match the simulated CBL depth, although the differences are relatively small when compared with the scatter in the LES estimates. In the GS-case CBL with $\partial\theta/\partial z = 0.010$ K m^{-1} and $Q_s = 0.10$ K m s^{-1} (Fig. 5b), the ZOM-predicted CBL depth z_i was actually a little closer to the simulated CBL depth (see Table 2). In Fig. 5c, the inherent deficiency of the ZOM-based entrainment in Eq. (25) is most obvious: the ZOM-predicted growth rate became unbounded or negative for the GC-case CBL, and the model could not be run to completion using an initialization earlier than approximately $t_0 = 15\,000$ s. Even at that time, the ZOM-predicted growth rate was unrealistically large for about 5000 s. It is noteworthy, however, that the FOM system of equations also predicts a larger than simulated entrainment rate for the same case. In several other cases, the FOM system of equations could be initialized at earlier stages of the CBL development than the ZOM system could. There were no cases in which the opposite was true. Although the FOM- and ZOM-based equations are both susceptible to numerical problems (see section 3b), the ZOM entrainment equation is more susceptible to these problems if the shear becomes strong enough. It appears that the inclusion of the finite entrainment zone thickness is beneficial to the bulk modeling of the CBL evolution in the presence of strong wind shears. However, when numerical problems are absent (which is typically the case of weakly sheared CBL), the ZOM appears to account for the integral properties of the sheared CBL nearly equally as well as the FOM.

For comparison, Fig. 6 shows the predictions of the bulk parameters of entrainment by the ZOM-based system of equations. Aside from the problems associated with the form of the entrainment in Eq. (25), the model predicted the simulated parameters of entrainment fairly well.

2) COMPARISON WITH PREVIOUSLY PROPOSED FOM VERSIONS

ML76 employed a number of simplifications, in their FOM, beyond those we have made in the present study. The most restrictive of these assumptions appears to be the omission of the entrainment zone thickness in their CBL integral velocity equations, see Eqs. (14) and (15) in ML76 versus our Eqs. (17) and (18) in section 2. Additionally, the dissipation parameterization in the ML76 TKE balance equation (20), provided some undesirable mathematical behavior of the system of equations, so we modified the ML76 TKE equation slightly as follows:

$$\frac{1}{2}C_P(\Delta u_1^2 + \Delta v_1^2)\frac{dz_i}{dt} + \frac{1}{2}B_s z_i - \frac{1}{2}\Delta b_1(z_i + \Delta z)\frac{dz_i}{dt} - C_{\varepsilon B}w_*^3 = 0, \quad (27)$$

with constants $C_P = C_{\varepsilon B} = 0.4$. The critical Richardson number constraint in (20) was used to determine the entrainment zone thickness.

Tests of the ML76 FOM revealed slightly lower CBL growth rates than both LES and the ZOM. A more significant difference, however, occurred in predictions of the buoyancy (Fig. 7) and velocity profiles. When the entrainment zone thickness is deleted from the buoyancy and velocity integral balance equations, the velocity and buoyancy equations revert to their ZOM counterparts, and this inconsistency with the FOM formulation, which ML76 retain in their TKE equation, results in excessive entrainment of buoyancy and momentum. Consequently, the parameters Δz, Δb_1, Δu_1, and Δv_1 remain small while the entrainment becomes excessively large, resulting in mixed-layer buoyancy and momentum being too large.

Recently, KPPV derived a more complex set of FOM equations for the CBL growth and tested those equations against LES data for six CBL cases that are very similar to the GC-case CBLs of the present study. The results of those tests show relatively good agreement between the KPPV LES- and FOM-based predictions of the integral parameters of entrainment. In CFII, we described tests of the KPPV entrainment zone heat flux parameterization, Eq. (26) in KPPV, and found reasonably good agreement for GS- and GC-case CBLs. A proper comparison between our FOM and the KPPV equations requires a more detailed investigation than is possible within the present study. Presumably, because

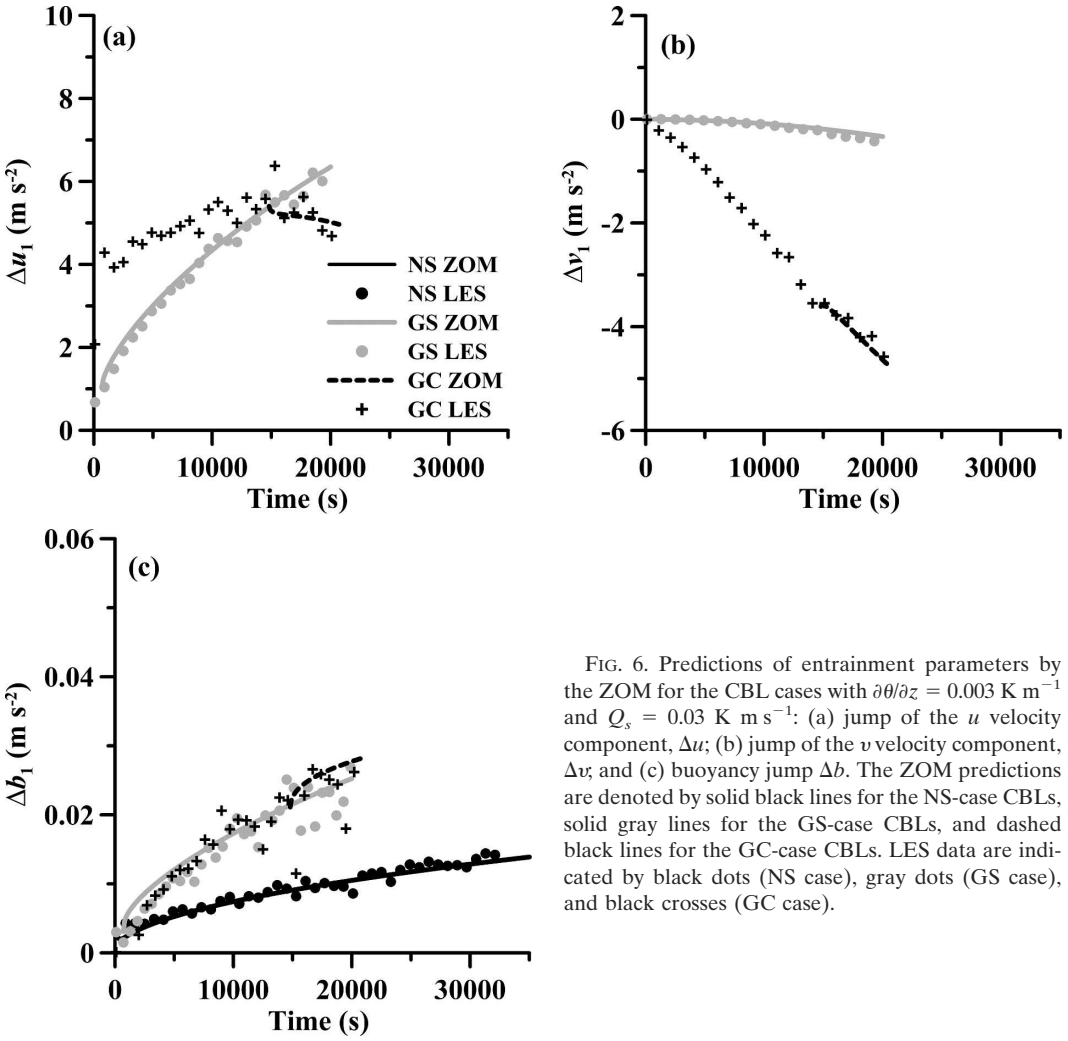

FIG. 6. Predictions of entrainment parameters by the ZOM for the CBL cases with $\partial\theta/\partial z = 0.003$ K m^{-1} and $Q_s = 0.03$ K m s^{-1}: (a) jump of the u velocity component, Δu; (b) jump of the v velocity component, Δv; and (c) buoyancy jump Δb. The ZOM predictions are denoted by solid black lines for the NS-case CBLs, solid gray lines for the GS-case CBLs, and dashed black lines for the GC-case CBLs. LES data are indicated by black dots (NS case), gray dots (GS case), and black crosses (GC case).

KPPV retain the entrainment zone thickness in their momentum equations, their equations should predict the evolution of the sheared CBL entrainment parameters more accurately than those of ML76. One possible point of departure of KPPV from our model is their inclusion of the friction velocity u_* in the TKE balance equation. This may affect the ability to model the differences between the GC- and GS-case CBLs in situations in which the two have similar shear at the CBL top and similar entrainment rates (see Fig. 3c). In such cases, the GC-case CBLs have a relatively large u_*, and the GS-case CBLs do not.

One assumption shared by ML76 and KPPV is that the buoyancy and velocity fluxes in the entrainment zone are linear, whereas (A10)–(A12) show the flux profiles to be quadratic in z. Our results indicate this assumption does not have a large effect on the modeled CBL growth. As an indication of this, the buoyancy flux profile in Fig. 2a is taken directly from FOM output for the GS case with $\partial\theta/\partial z = 0.003$ K m^{-1} and $Q_s = 0.03$ K m s^{-1}. Some slight curvature is present, but the profile could be represented reasonably well by a linear function.

c. *Sensitivity of FOM predictions to entrainment zone Ri_g*

LES results (CFI) have shown that the gradient Richardson number

$$\mathrm{Ri}_g = \frac{N^2}{\left(\frac{\partial u}{\partial z}\right)^2 + \left(\frac{\partial v}{\partial z}\right)^2},$$

and especially the flux Richardson number

$$\mathrm{Ri}_f = \frac{-B}{\tau_x \frac{\partial u}{\partial z} + \tau_y \frac{\partial v}{\partial z}},$$

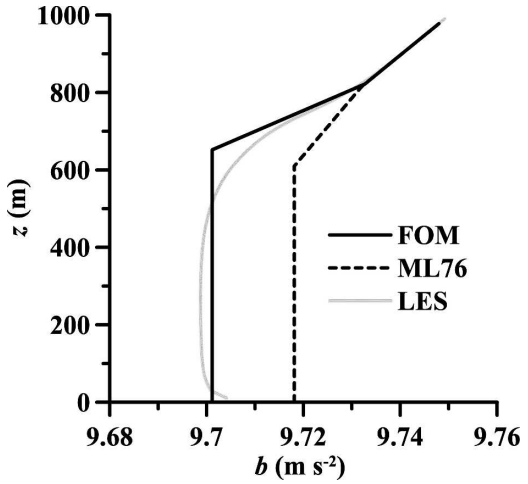

FIG. 7. Comparison of predicted buoyancy profiles at $t = 10\,000$ s for the GS-case CBL with $\partial\theta/\partial z = 0.003$ K m^{-1} and$Q_s = 0.03$ K m s^{-1}. The dashed black line corresponds to the FOM-based equations based on ML76, the solid black line represents the FOM of the present study, and the solid gray line is the LES profile.

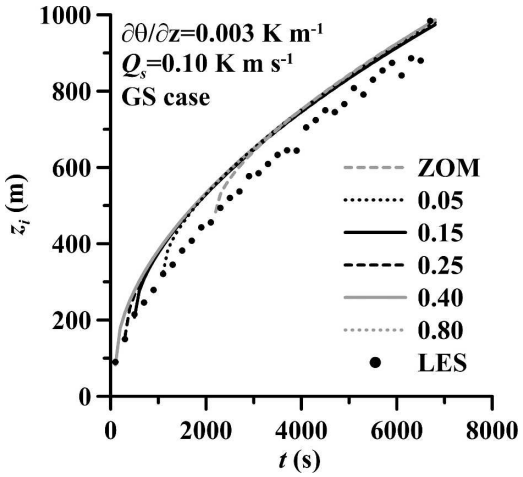

FIG. 8. Dependence of the CBL depth z_i on the choice of the critical Ri_1 value for the GS-case CBL with $\partial\theta/\partial z = 0.003$ K m^{-1} and $Q_s = 0.1$ K m s^{-1}. Results for five critical Ri_1 values are shown: 0.05 (black dotted line), 0.15 (black solid line), 0.25 (black dashed line), 0.4 (gray solid line), and 0.8 (gray dotted line). Shown also for comparison are the ZOM (gray dashed line) and LES data (black dots).

become constant in the entrainment zone of sheared CBLs when the shear becomes a large contributor to the entrainment zone TKE. Nevertheless, with horizontal averaging involved (section 2c), Ri_g and Ri_f can take on large values in the entrainment zone when the shear is relatively weak. In such cases, the meaning of Ri_g and Ri_f for bulk modeling of sheared CBLs becomes less clear, and the issue of how to parameterize their behavior in the entrainment zone is not settled. Thus, we wish to explore in this section the impact of different parameterizations of entrainment zone Ri on the FOM predictions of CBL evolution. These different parameterizations include alternative choices for the critical value of Ri_1, incorporating w_* in the denominator of (20), as well as using a variable Richardson number in place of constant bulk Ri_1.

1) SENSITIVITY TO THE VALUE OF Ri_1

The FOM model runs presented in section 4a have been conducted adopting $\mathrm{Ri}_1 = 0.15$. Choosing a value this low, at first, may seem too restrictive and inconsistent with both LES data (Otte and Wyngaard 2001; CFI) and atmospheric measurements (ML76), which demonstrate Ri values closer to 0.25. However, the value $\mathrm{Ri}_1 = 0.15$ in (20) provides FOM predictions most consistent with LES results, at least within the context of our analysis. In this section, we explain the reason for this apparent discrepancy and explore the impact of different choices of the critical Ri value on the modeled entrainment zone parameters.

As Ri_1 approaches zero, the entrainment zone depth decreases, and the FOM representation of the CBL structure approaches that of the ZOM, so the behavior of the FOM in such circumstances approaches that of the ZOM, and the FOM-predicted integral parameters of entrainment closely match their ZOM counterparts. A rather interesting behavior occurs if Ri_1 approaches Ri_g of the background atmospheric profile. In that case, the TKE balance becomes more difficult to achieve, and the entrainment zone depth becomes very large. If $\mathrm{Ri}_1 > \mathrm{Ri}_g$, the FOM system of equations becomes unbalanced and has no solution. Interestingly, the CBL depth z_i is not greatly affected by Ri_1 changes. In fact, plots of z_i versus t for different Ri_1 values generally overlap to the extent that the reader would not be able to discern significant differences among them. The only exception is for cases of small Ri_1 in which instability occurs (Fig. 8). The relative insensitivity of z_i is perfectly consistent with the fact that z_i predictions of the ZOM and FOM are generally rather close (Fig. 5). The largest impact of perturbing Ri_1 is on the entrainment zone parameters and mixed-layer velocity and buoyancy. As Ri_1 increases, the entrainment zone depth increases (Fig. 9), and the buoyancy and velocity increments increase correspondingly. Likewise, entrainment rates of buoyancy and velocity increase, and these increases are reflected in greater mixed-layer values.

Although the FOM does not explicitly predict TKE as a dependent variable, larger TKE values are necessary to achieve the momentum and buoyancy balance required for the mixed-layer values to increase. Since

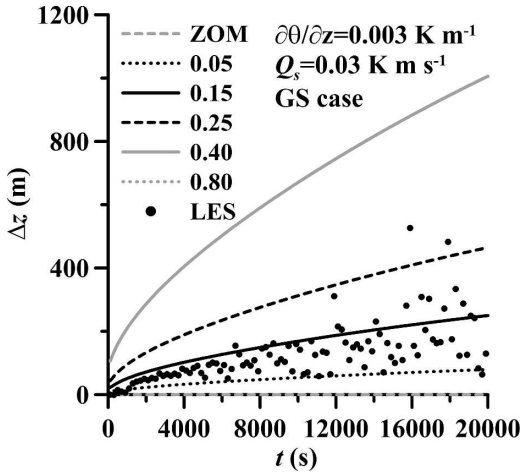

FIG. 9. Dependence of the FOM entrainment zone thickness Δz on the critical Ri_1 value for the GS-case CBL with $\partial\theta/\partial z = 0.003$ K m^{-1} and $Q_s = 0.03$ K m s^{-1}. Results for five critical Ri_1 values are shown: 0.05 (black dotted line), 0.15 (black solid line), 0.25 (black dashed line), 0.4 (gray solid line), and 0.8 (gray dotted line). Shown also for comparison are the ZOM (gray dashed line) and LES data (black dots). The LES data were obtained using the integral buoyancy-conserving technique described in CFII.

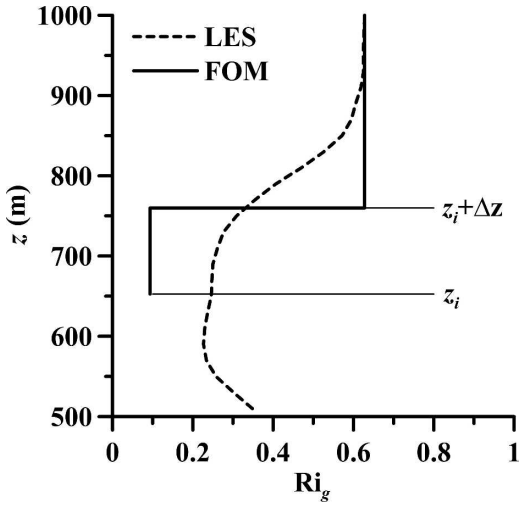

FIG. 10. Gradient Richardson number Ri_g vs height z at $t = 10\,000$ s for the GS-case CBL with $\partial\theta/\partial z = 0.003$ K m^{-1} and $Q_s = 0.03$ K m s^{-1} retrieved from LES: directly from horizontally averaged profiles of u, v, and b (dashed line) and within the FOM framework using the integral buoyancy-conserving technique from CFII (thick solid line). The horizontal thin lines indicate the CBL depth z_i and the top of the FOM entrainment zone $z_i + \Delta z$.

the independent variables B_s, N, Γ_u, Γ_v, f, and C_D are the same among all test runs, only the difference in TKE can explain observed changes in modeled mixed-layer momentum and buoyancy. That is, as seen from (A7), (A8), and (A9), larger mixed-layer values require larger negative turbulent fluxes at the CBL top, and larger turbulent fluxes require more TKE. We find, therefore, that Ri_1 acts as a regulator for the CBL and entrainment zone integral TKE. It acts to impose a capping value on the integral TKE in the FOM representation of the mixed layer and entrainment zone. If in the FOM $\mathrm{Ri}_1 < 0.15$ (our standard value adopted for critical Ri), the entrainment zone depth increases, and upon reaching $\mathrm{Ri}_1 = 0.15$, an entrainment zone TKE balance is achieved in which generation by shear is balanced by dissipation and buoyancy destruction. If $\mathrm{Ri}_1 > 0.15$, the conditions in the modeled entrainment zone are generally turbulence suppressing, and the entrainment zone collapses so that $\mathrm{Ri}_1 = 0.15$.

Figure 10 gives an idea why $\mathrm{Ri}_1 = 0.15$ provides the overall best agreement between LES and FOM predictions (although individual cases might have different degrees of agreement). We show Ri_g values for the LES profiles in Fig. 2 compared with the FOM profiles retrieved from the LES data for the corresponding time step. The FOM-specific analysis procedure (CFII) defines the mixed-layer values as the vertical averages below $z = z_i$ and requires conservation of buoyancy between the LES and the retrieved FOM profiles. Because the FOM mixed-layer values are required to be height constant, the shear and buoyancy gradients must be concentrated in the entrainment zone in order for integral buoyancy and momentum to be the same in FOM and LES. As a consequence of these restrictions, the FOM Ri_g is undefined in the mixed layer whereas in LES, it is positive at least in the upper portion of the mixed layer. In the entrainment zone, the FOM Ri_g is 0.09, whereas the LES Ri_g is 0.25. In the quiescent-free atmosphere well above the CBL, both FOM and LES have the same Ri_g.

The presented analysis demonstrates an inconsistency between the LES horizontally averaged CBL structure and its representation in the FOM. The realistic LES mixed layer is not perfectly mixed. This can be regarded as a deficiency in the mixed-layer modeling approach, but it is a simplification that is necessary to make bulk models tractable. Nevertheless, we feel that the analysis method we have chosen represents the fairest comparison between LES and FOM, and the value $\mathrm{Ri}_1 = 0.15$ provides the closest match between LES and FOM predictions. Outside of the restrictions of the above analysis procedure, other critical Ri values such as 0.25 can be considered equally appropriate, and any user of the presented FOM might prefer to use such values instead.

2) OTHER FORMULATIONS OF Ri_1

Sorbjan (2004) has suggested a parameterization of the heat flux minimum in the entrainment zone of baro-

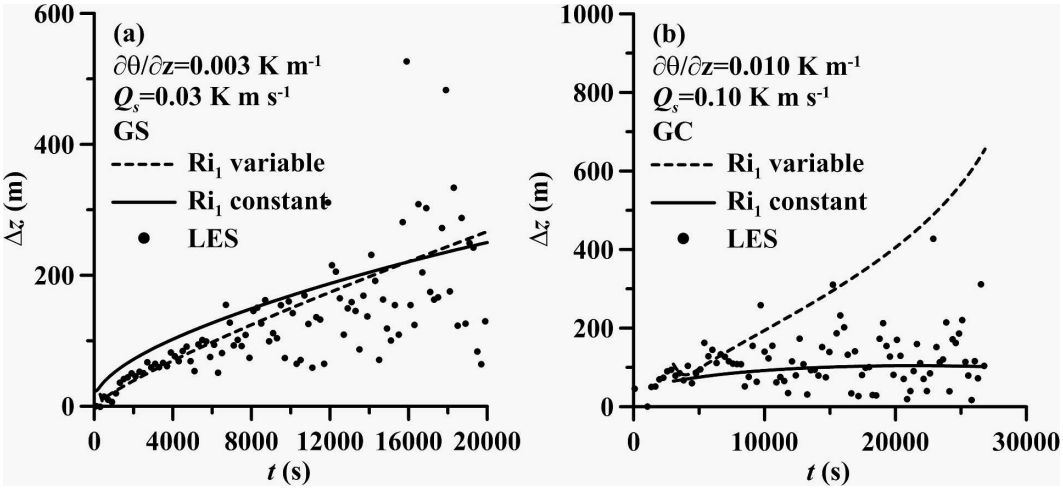

FIG. 11. The FOM entrainment zone thickness Δz as a function of time t for the following CBL cases: (a) GS case with $\partial\theta/\partial z = 0.003$ K m^{-1} and $Q_s = 0.03$ K m s^{-1}; (b) GC case with $\partial\theta/\partial z = 0.010$ K m^{-1} and $Q_s = 0.1$ K m s^{-1}. The solid lines correspond to the FOM equations with $\mathrm{Ri}_1 = 0.15$, the dashed lines correspond to the FOM using the Sorbjan (2004) entrainment zone heat flux parameterization, and the dots are LES data retrieved using the integral buoyancy-conserving technique (CFII).

clinic CBLs. We tested a version of the FOM equations with this parameterization in order to allow the entrainment zone Ri to vary in time with the other parameters. If we combine Eq. (23b) of Sorbjan (2004) with (A10), the heat flux at $z = z_i$ becomes

$$B(z_i) = B_s - z_i\left[N^2\frac{d}{dt}(z_i + \Delta z) - \frac{d\Delta b_1}{dt}\right] = c_H w_*^2\left(\frac{\Delta b_1}{\Delta z}\right)^{1/2}\frac{(1 + c_2/\mathrm{Ri}_1)}{(1 + 1/\mathrm{Ri}_1)^{1/2}}, \quad (28)$$

with $c_2 = 1.5$ and $c_H = 0.015$. The value of c_H is doubled from its value in Sorbjan (2004) because the larger value agreed better with LES data (see CFII). In addition, we modified (20) to allow time-varying Ri_1 behavior:

$$\frac{d\mathrm{Ri}_1}{dt} = \frac{d}{dt}\left(\frac{\Delta b_1 \Delta z}{\Delta u_1^2 + \Delta v_1^2}\right). \quad (29)$$

Tests of (28) and (29) in place of (20) did not bring about any improvement in the FOM predictions of entrainment parameters. As in other tests, the prediction of z_i did not change much, but the entrainment zone thickness Δz and corresponding velocity and buoyancy jumps were rather strongly affected in some cases. Agreement was reasonably good in cases with weaker background vertical buoyancy gradients but much poorer for larger stratification (see Fig. 11). We found that Ri_1 always increased with time in this version of the FOM, whereas in LES, Ri_g trended toward a constant value (CFI). While the Sorbjan (2004) parameterization performs exceptionally well when compared in a diagnostic manner against LES data, it does not work well in a prognostic setting. We feel that such a result may be a reflection of the difference between LES and FOM profiles of buoyancy flux (see Fig. 2). The Sorbjan (2004) parameterization is specific to LES profiles, which do not feature such a sharp buoyancy flux minimum in the entrainment zone, and some additional work would be necessary to bring it into a FOM-specific framework.

One could also consider Eq. (30) from KPPV, which expresses the entrainment zone thickness in terms of another Richardson number:

$$\frac{\Delta z}{z_i} = a\mathrm{Ri}_K^{-1} + b, \quad (30)$$

where

$$\mathrm{Ri}_K = \frac{\Delta b_1 z_i}{w_*^2 + cu_*^2 + d(\Delta u_1^2 + \Delta v_1^2)}, \quad (31)$$

and a, b, c, and d are constants. However Ri_K, which employs z_i in place of Δz, is not specific to the entrainment zone and is therefore not a simple substitute for Ri_1 in our study. Like the Sorbjan (2004) parameterization, KPPV works well within its specific framework, but some additional work is needed to make it compatible with (16)–(19).

3) INCORPORATION OF CONVECTIVE VELOCITY SCALE IN Ri_1

The observed finiteness of the entrainment zone depth in the shear-free CBL might seem inconsistent with the proposed bulk model where the entrainment zone of finite depth arises only in the presence of mean shear across the CBL top. In an attempt to resolve this inconsistency, we explored the effect of incorporating the convective velocity scale w_* in the formulation for Ri_1 in order to parameterize the finite depth of the entrainment zone in shear-free conditions. The modified version of (20) was

$$\mathrm{Ri}_1 = \frac{\Delta b_1 \Delta z}{\Delta u_1^2 + \Delta v_1^2 + w_*^2}. \tag{32}$$

Tests of (32) against shear-free CBLs (where the effects of w_* should be strongest), shown in Fig. 12, revealed that the modeled entrainment zone thickness was considerably less than the LES-retrieved entrainment zone thickness (see CFII). Attempts to increase the entrainment zone thickness by adding a constant in front of w_* did not improve the performance of the parameterization against LES data. The use of (32) also does not lead to an understanding of why the ZOM equations (21)–(24) are able to model $z_i(t)$ so well in shear-free cases. Thus, for the reasons stated in section 2, we opted to omit w_* from our entrainment zone thickness equation in the FOM.

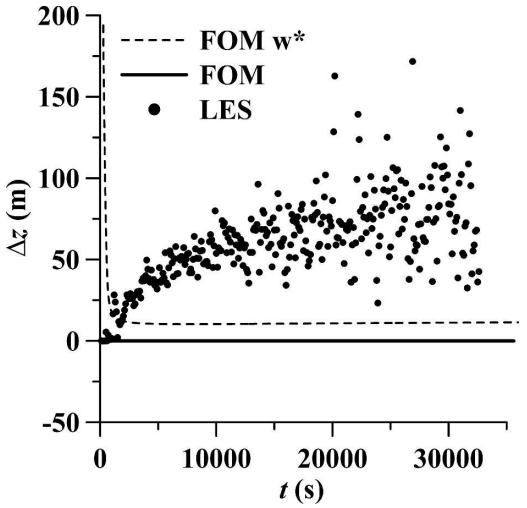

FIG. 12. The entrainment zone thickness Δz for the shear-free (NS case) CBL with $\partial\theta/\partial z = 0.003$ K m^{-1} and $Q_s = 0.03$ K m s^{-1}, predicted by a version of the FOM that was modified to include the convective velocity scale w_* in the definition of Ri_1 (dashed line). The prediction is compared with the version of the FOM without w_* in the expression of Ri_1 (solid line) and LES data (dots). The LES-predicted Δz was retrieved using the integral buoyancy-conserving technique explained in CFII.

d. Sensitivity to C_P

Here we address the sensitivity of the FOM predictions to C_P, that is, the fraction of entrainment zone shear-produced TKE consumed by entrainment. Analysis of LES results (CFI) and tests of entrainment parameterizations (CFII) have both shown that a value $C_P = 0.4$ is most consistent with LES data. Results of tests using $C_P = 0.25$, $C_P = 0.4$, and $C_P = 0.7$ on the modeled CBL evolution for the CBL cases with $\partial\theta/\partial z = 0.003$ K m^{-1} and $Q_s = 0.03$ K m s^{-1} are presented in Fig. 13. The case with $C_P = 0.7$ could not be displayed in Fig. 13a because of numerical instabilities [see Eq. (26)]. With $C_P = 0.25$, the modeled CBL grew a bit more slowly than the simulated one, but the difference was not as remarkable as with $C_P = 0.7$, probably because with $C_P = 0.7$, the system of equations was either unstable or nearly unstable, and modeled growth rates increased more dramatically. This general behavior is consistent among the other cases. A smaller value of C_P means that less of the shear-produced TKE is available for the negative buoyancy flux of entrainment, and the CBL grows more slowly. In cases with stronger stratification, the turbulence-suppressing effects of buoyancy reduce the sensitivity to C_P, whereas in more weakly stratified cases, the FOM is more likely to become unstable as C_P is increased. In general, over all cases simulated, the modeled CBL growth with $C_P = 0.4$ is most consistent with the simulated CBL growth.

5. Summary and conclusions

In this study, a new set of bulk model equations based on the first-order model (FOM) representation of the sheared CBL structure has been derived. Entrainment predictions by these equations have been tested against a dataset from 24 LES runs for CBLs with three different wind shear configurations [no shear (NS), height-constant geostrophic forcing (GC), and linear geostrophic shear (GS)] and compared with a set of (zero-order model) ZOM-based equations. From the tests of the both parameterizations, the following conclusions were reached with respect to the questions listed in section 1.

1) The investigated behavior of the FOM- and ZOM-based entrainment equations shows that the entrainment zone of finite thickness Δz is an important feature of the entrainment process to be accounted for in bulk models of entrainment for sheared CBLs.

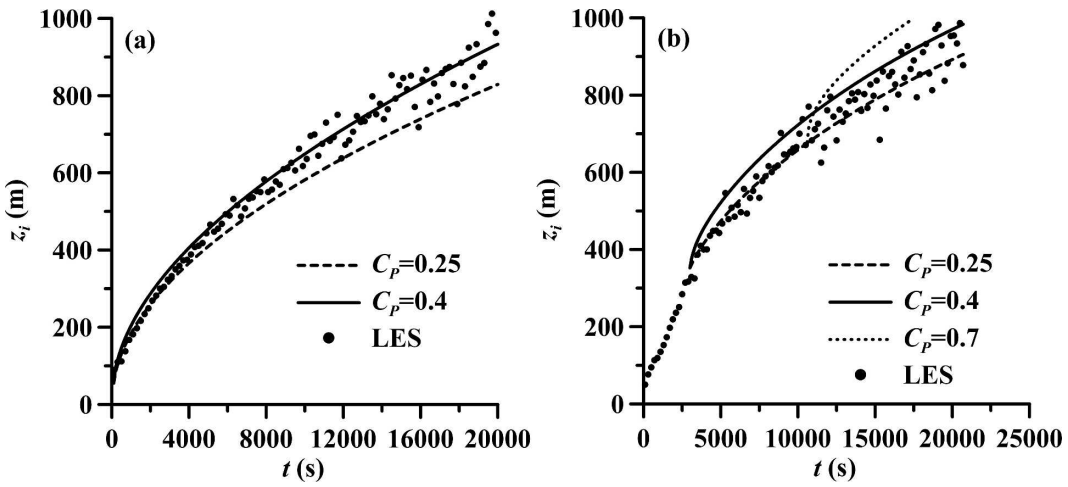

FIG. 13. CBL depth z_i as a function of time t for the FOM using different values of the constant C_P for the CBL cases with $\partial\theta/\partial z = 0.003$ K m^{-1} and $Q_s = 0.03$ K m s^{-1}: (a) GS and (b) GC case. The dashed lines correspond to $C_P = 0.25$, solid lines correspond to $C_P = 0.4$, the dotted lines represent $C_P = 0.7$, and the dots represent LES data.

The FOM clearly appears to be superior to the ZOM for modeling the sheared CBL. In many cases, however, the ZOM was found capable of quantifying the integral shear production of turbulence and its effects on the CBL evolution almost as successfully as the FOM despite its more simplified representation of the CBL structure. The advantage of the FOM is primarily manifested by its ability to largely mitigate the instability inherent in the ZOM entrainment equation. Despite this apparent advantage, the instability can still occur in the FOM entrainment equation, although such occurrences seem to be mostly limited to cases in which the shear in the background atmospheric profile is too strong to guarantee stability, in the Kelvin–Helmholtz sense, to finite perturbations.

2) The entrainment zone thickness in the proposed FOM is governed by the choice of critical value of Ri_1. As this value approaches zero, the FOM reverts to the ZOM. If it equals or exceeds the value of the atmospheric background Ri_g (in a linearly stratified atmosphere), the FOM equations have no solution. In between these two extremes, the impact of increasing Ri_1 is to increase the entrainment zone depth, with the buoyancy and velocity increments increasing correspondingly, whereas the CBL depth z_i remains relatively unaffected. As a consequence, the entrainment of buoyancy and velocity into the mixed layers increases, resulting in their increased mixed-layer values compared to those with a smaller Ri_1. The critical value of Ri_1 controls the entrainment of buoyancy and velocity into the mixed layer and acts as a valve in the TKE generation in the entrainment zone. Overall, we find that using $\mathrm{Ri}_1 = 0.15$ provides the best match with LES data. However, this particular value is partly a result of the analysis procedure designed to bring LES profiles into the FOM framework. The reader may well consider other critical values of Ri_1 to be appropriate.

   The role of the entrainment zone Ri_g in the CBL bulk modeling is still an open question. In particular, in the limit of the entrainment zone shear approaching zero, horizontally averaged Ri_g from LES may be much larger than 0.25 (Sorbjan 2004). It needs to be determined to what extent this behavior is due to undulating motions of the entrainment interface and to what extent it is a reflection of a diffused interface.

3) Results of the conducted tests lend further evidence to support the finding (reported in detail in CFI and CFII) that the surface shear production of TKE does not directly affect the entrainment process, and the corresponding terms may be omitted in the bulk model TKE budget (entrainment) equations. However, the shear-related terms have been retained in the momentum balance equations. The tests of these equation sets have shown good agreement between the modeled and simulated parameters of entrainment. Although we present no results on the sensitivity of the equations to the parameterization of surface shear in the integral TKE equation, our attempts to include this term in the TKE equation only resulted in poorer agreement with LES data. In none of the GC cases did we find that the entrainment rate was underpredicted by omitting the surface shear term from the TKE equation.

The performed tests have also shown that physical meaning of the nonstationary term in the integral TKE balance equations needs to be reconsidered. We have found better agreement between our model and LES data when the nonstationary term has been omitted. Our present thinking is that the combination of the nonstationary term with the integral dissipation term in the TKE budget represents a net sink of TKE, which is well quantified by a scaled dissipation term alone in the regime of equilibrium entrainment (Fedorovich et al. 2004a). As Fedorovich et al. (2004b) have demonstrated, scaled integral TKE and dissipation strongly vary with time at early stages of the CBL growth or when the developing CBL encounters rapidly changing potential temperature stratification at its top.

The proposed entrainment parameterizations obviously need additional testing against atmospheric data. Atmospheric data that have been analyzed to date for this purpose (see, e.g., ML76) suggest, however, that the balance between shear generation and buoyancy destruction of turbulence in the entrainment zone, adopted in the present study as a key entrainment parameterization concept, appears to be a consistent feature of the entrainment process in the atmospheric CBL.

Acknowledgments. This work has been supported by National Science Foundation Grant ATM-0124068, and the first author was funded by National Science Foundation Grant ATM-0305412 while completing the research related to this paper. He would like to thank members of his Ph.D. advisory committee, Charles A. Doswell III, Brian Fiedler, Randall Kolar, Douglas Lilly, and Alan Shapiro, for their insightful comments on this study. The authors would also like to thank the four anonymous reviewers whose suggestions greatly helped to improve this manuscript.

APPENDIX

Derivation of FOM Integral Momentum, Buoyancy, and TKE Budgets

The FOM integral momentum, buoyancy, and TKE budgets are obtained in the same manner as the ZOM budgets (Fedorovich 1995; CFII), except that the upper limit of the vertical integration is the upper limit of the entrainment zone ($z_i + \Delta z$) rather than z_i adopted as the CBL top in the ZOM. In the FOM-related equations below, the subscript "1" is added to represent FOM parameters of entrainment where they differ from the corresponding ZOM parameters.

In the mixed layer, the buoyancy is constant with height [$b = b_{m1}(t)$], and Eq. (1), integrated over the depth of the mixed layer, gives

$$\int_0^{z_i} \frac{\partial b}{\partial t}\, dz = z_i \frac{db_{m1}}{dt} = B_s - B_{i1}. \tag{A1}$$

In the entrainment zone, buoyancy is a linear function of height: $b(z, t) = b_{m1}(\mathrm{t}) + [\Delta b(t)/\Delta z(t)][z - z_i(t)]$, and the resulting integral entrainment zone buoyancy balance equation is

$$\int_{z_i}^{z_i + \Delta z} \frac{\partial b}{\partial t}\, dz = \Delta z \frac{db_{m1}}{dt} + \frac{1}{2}\frac{d}{dt}(\Delta b_1 \Delta z) - \Delta b_1 \frac{d}{dt}(z_i + \Delta z) = B_{i1}. \tag{A2}$$

We then add (A1) and (A2) and use the relation

$$\frac{db_{m1}}{dt} = \frac{d}{dt}[N^2(z_i + \Delta z) - \Delta b_1], \tag{A3}$$

where N is the Brunt–Väisälä frequency of the background atmospheric profile, to arrive at the integral buoyancy balance equation:

$$\frac{d}{dt}\left[\frac{N^2(z_i + \Delta z)^2}{2} - \Delta b_1\left(z_i + \frac{\Delta z}{2}\right)\right] = B_s, \tag{A4}$$

which is (5) in section 2b.

The left-hand sides of both (2) and (3), as well as the first terms on the right-hand sides of those equations, are of the same form as corresponding terms in (1). Like the buoyancy b, the velocity components u and υ are assumed to be constant in the mixed layer and are linear functions of height z in the entrainment zone. The geostrophic parts of the velocity components u and υ may be approximated as $u_g = u_s + \Gamma_u z$ and $\upsilon_g = \upsilon_s + \Gamma_\upsilon z$, respectively (Fedorovich 1995). When terms with the Coriolis parameter are integrated from the surface to the upper limit of the entrainment zone and added to the respective flux terms of (2) and (3), their sums yield the integral budget equations for the velocity components:

$$\frac{d}{dt}\left[\frac{\Gamma_u(z_i + \Delta z)^2}{2} - \Delta u_1\left(z_i + \frac{\Delta z}{2}\right)\right] = -\tau_{xs} + f\left[\frac{\Gamma_\upsilon(z_i + \Delta z)^2}{2} - \Delta \upsilon_1\left(z_i + \frac{\Delta z}{2}\right)\right], \tag{A5}$$

$$\frac{d}{dt}\left[\frac{\Gamma_\upsilon(z_i + \Delta z)^2}{2} - \Delta \upsilon_1\left(z_i + \frac{\Delta z}{2}\right)\right] = -\tau_{ys} - f\left[\frac{\Gamma_u(z_i + \Delta z)^2}{2} - \Delta u_1\left(z_i + \frac{\Delta z}{2}\right)\right], \tag{A6}$$

which are (6) and (7), respectively, in section 2b.

The first step in deriving the integral budget of TKE is to integrate the buoyancy and velocity balance equations (1)–(3) up to some arbitrary level z to obtain the flux profiles. In the mixed layer, at $0 \le z \le z_i$, these profiles have the following form:

$$B(z) = B_s - z\frac{db_{m1}}{dt}, \tag{A7}$$

$$-\tau_x(z) = -\tau_{xs} - z\frac{du_{m1}}{dt} + f\left\{[\Gamma_\upsilon(z_i + \Delta z) - \Delta\upsilon_1]z - \Gamma_\upsilon\frac{z^2}{2}\right\}, \tag{A8}$$

$$-\tau_y(z) = -\tau_{ys} - z\frac{d\upsilon_{m1}}{dt} - f\left\{[\Gamma_u(z_i + \Delta z) - \Delta u_1]z - \Gamma_u\frac{z^2}{2}\right\}. \tag{A9}$$

In the entrainment zone, at $0 \le z \le z_i + \Delta z$, the profiles are

$$B(z) = B_s - z\frac{db_{m1}}{dt} - \frac{d}{dt}\left[\frac{\Delta b_1}{\Delta z}\frac{(z - z_i)^2}{2}\right], \tag{A10}$$

$$-\tau_x(z) = -\tau_{xs} - z\frac{du_{m1}}{dt} - \frac{d}{dt}\left[\frac{\Delta u_1}{\Delta z}\frac{(z - z_i)^2}{2}\right] + f\left\{[\Gamma_\upsilon(z_i + \Delta z) - \Delta\upsilon_1]z - \Gamma_\upsilon\frac{z^2}{2}\right\} + f\frac{\Delta\upsilon_1}{\Delta z}\frac{(z - z_i)^2}{2}, \tag{A11}$$

$$-\tau_y(z) = -\tau_{ys} - z\frac{d\upsilon_{m1}}{dt} - \frac{d}{dt}\left[\frac{\Delta\upsilon_1}{\Delta z}\frac{(z - z_i)^2}{2}\right] - f\left\{[\Gamma_u(z_i + \Delta z) - \Delta u_1]z - \Gamma_u\frac{z^2}{2}\right\} - f\frac{\Delta u_1}{\Delta z}\frac{(z - z_i)^2}{2}. \tag{A12}$$

Integrating (A7) over the mixed-layer depth and (A10) over the entrainment zone depth, adding the two, then using (A3) to eliminate db_{m1}/dt, we find the buoyancy flux contribution to the integral TKE budget:

$$\int_0^{z_i + \Delta z} B\,dz = \frac{1}{2}B_s(z_i + \Delta z) - \frac{1}{2}z_i\Delta b_1\frac{dz_i}{dt} + \frac{1}{4}\left(z_i + \frac{\Delta z}{3}\right)\left(\Delta z\frac{d\Delta b_1}{dt} - \Delta b_1\frac{d\Delta z}{dt}\right), \tag{A13}$$

which is the same as (10) in section 2b. The first two terms of (A13) are nearly identical in form to the corresponding terms in the ZOM integral TKE equation [see Eq. (21) in Fedorovich 1995 and Eq. (8) of CFII] except that Δz is added to the first term. The last term arises from the fact that the expression $\Delta b_1(dz_i/dt)$ is not an exact representation of $-B_{i1}$ (the buoyancy flux at $z = z_i$) as its ZOM counterpart $B_{i0} = -\Delta b dz_i/dt$ is. No such simplifications are made here.

The contribution of shear generation of turbulence to the integral TKE budget is obtained by integrating the first two terms on the right-hand side of (4). This integration is simplified by the fact that the shear is zero in the mixed layer. The surface layer contribution to the shear term has the same form as in the ZOM (Fedorovich 1995) and is given by $u_{m1}\tau_{xs} + \upsilon_{m1}\tau_{ys}$. To obtain the entrainment zone shear contribution, we integrate (A11) and (A12) from $z = z_i$ to $z = z_i + \Delta z$, taking special care with the integration of the third term on the right-hand sides of both equations. We then multiply the u-component integral by $\partial u/\partial z = \Delta u_1/\Delta z$ and the υ-component integral by $\partial\upsilon/\partial z = \Delta\upsilon_1/\Delta z$ (this can be done after the integration because Δu_1, $\Delta\upsilon_1$, and Δz are not functions of z) to obtain the integral shear TKE production in the entrainment zone. Finally, the relations $u_{m1} = u_s + \Gamma_u(z_i + \Delta z) - \Delta u_1$ and $\upsilon_{m1} = \upsilon_s + \Gamma_\upsilon(z_i + \Delta z) - \Delta\upsilon_1$ are used to eliminate the mixed-layer velocity components. The resulting equation describing the integral shear generation of TKE in the FOM of CBL reads

$$\int_0^{z_i + \Delta z} S\,dz = [u_s + \Gamma_u(z_i + \Delta z) - \Delta u_1]\tau_{xs} + [\upsilon_s + \Gamma_\upsilon(z_i + \Delta z) - \Delta\upsilon_1]\tau_{ys} + \frac{1}{2}(\Delta u_1^2 + \Delta\upsilon_1^2)\frac{d}{dt}\left(z_i + \frac{2}{3}\Delta z\right) + \frac{\Delta z}{12}\frac{d}{dt}(\Delta u_1^2 + \Delta\upsilon_1^2) - \frac{\Delta z}{2}(\Gamma_u\Delta u_1 + \Gamma_\upsilon\Delta\upsilon_1)\frac{d}{dt}(z_i + \Delta z) + f\frac{\Delta z^2}{6}(\Gamma_\upsilon\Delta u_1 - \Gamma_u\Delta\upsilon_1), \tag{A14}$$

which is the same as (9) in section 2b. The third line of (A14) represents the shear generation of TKE due to the entrainment of momentum and has a similar form to the ZOM-based entrainment zone shear generation term, except for the $d(2\Delta z/3)/dt$ term, which essentially amounts to an adjustment for the fact that the param-

eterizations of the entrainment of velocity, $\tau_{xi} = \Delta u_1(dz_i/dt)$ and $\tau_{yi} = \Delta v_1(dz_i/dt)$, are not exact expressions in the FOM as their ZOM counterparts are (Fedorovich 1995). The fourth and fifth lines result from the inclusion of the entrainment zone depth as a parameter in the bulk model.

Because the turbulence time scale is so much shorter than the Coriolis time scale, the last term on the right-hand side of (A14) may seem a bit counterintuitive at first. Physically, the term represents the Coriolis effects on the velocity in the entrainment zone, and since the velocity profiles affect the shear generation of TKE, the Coriolis parameter does have an indirect effect on the shear generation of TKE in the entrainment zone.

The transport term, which is the fourth term on the right-hand side of (4), is assumed not to contribute to the integral TKE budget because the component of velocity normal to the rigid lower boundary is zero, there are no fluxes of TKE at $z = 0$. Furthermore, Stull (1976b) and Fedorovich et al. (2004a) have demonstrated that these fluxes at the top of the entrainment zone, where turbulence decays to zero, can be neglected under typical conditions in the atmospheric CBL. In the FOM, the turbulence decay to zero occurs at $z = z_i + \Delta z$.

REFERENCES

Ball, F. K., 1960: Control of inversion height by surface heating. *Quart. J. Roy. Meteor. Soc.,* **86,** 483–494.

Batchvarova, E., and S.-E. Gryning, 1991: Applied model for the growth of the daytime mixed layer. *Bound.-Layer Meteor.,* **56,** 261–274.

——, and ——, 1994: An applied model for the height of the daytime mixed layer and the entrainment zone. *Bound.-Layer Meteor.,* **71,** 311–323.

Betts, A. K., 1973: Non-precipitating cumulus convection and its parameterization. *Quart. J. Roy. Meteor. Soc.,* **99,** 178–196.

——, 1974: Reply to comment on the paper "Non-precipitating cumulus convection and its parameterization." *Quart. J. Roy. Meteor. Soc.,* **100,** 469–471.

Boers, R., E. W. Eloranta, and R. L. Coulter, 1984: Lidar observations of mixed layer dynamics: Tests of parameterized entrainment models of mixed layer growth rate. *J. Climate Appl. Meteor.,* **23,** 247–266.

Carson, D. J., 1973: The development of dry inversion-capped convectively unstable boundary layer. *Quart. J. Roy. Meteor. Soc.,* **99,** 450–467.

Conzemius, R., and E. Fedorovich, 2006a: Dynamics of sheared convective boundary layer entrainment. Part I: Methodological background and large eddy simulations. *J. Atmos. Sci.,* **63,** 1151–1178.

——, and ——, 2006b: Dynamics of sheared convective boundary layer entrainment. Part II: Evaluation of bulk model predictions of entrainment flux. *J. Atmos. Sci.,* **63,** 1179–1199.

Deardorff, J. W., 1970: Convective velocity and temperature scales for the unstable planetary boundary layer and for Raleigh convection. *J. Atmos. Sci.,* **27,** 1211–1213.

——, 1979: Prediction of convective mixed-layer entrainment for realistic capping inversion structure. *J. Atmos. Sci.,* **36,** 424–436.

Driedonks, A. G. M., 1982: Models and observations of the growth of the atmospheric boundary layer. *Bound.-Layer Meteor.,* **23,** 283–306.

Fedorovich, E., 1995: Modeling the atmospheric convective boundary layer within a zero-order jump approach: An extended theoretical framework. *J. Appl. Meteor.,* **34,** 1916–1928.

——, 1998: Bulk models of the atmospheric convective boundary layer. *Buoyant Convection in Geophysical Flows,* E. J. Plate et al., Eds., Kluwer, 265–290.

——, and D. V. Mironov, 1995: A model for a shear-free convective boundary layer with parameterized capping inversion structure. *J. Atmos. Sci.,* **52,** 83–95.

——, R. Conzemius, and D. Mironov, 2004a: Convective entrainment into a shear-free, linearly stratified atmosphere: Bulk models reevaluated through large eddy simulations. *J. Atmos. Sci.,* **61,** 281–295.

——, ——, and A. M. Shapiro, 2004b: Nonstationarity of convective boundary layer growth in a heterogeneously stratified, shear-free atmosphere. Preprints, *16th Symp. on Boundary Layers and Turbulence,* Portland, ME, Amer. Meteor. Soc., CD-ROM, 7.9.

García, J. A., M. L. Cancillo, and J. L. Cano, 2002: A case study of the morning evolution of the convective boundary layer depth. *J. Appl. Meteor.,* **41,** 1053–1059.

Garratt, J. R., 1992: *The Atmospheric Boundary Layer*. Cambridge University Press, 316 pp.

Haltiner, G. J., and R. T. Williams, 1980: *Numerical Prediction and Dynamic Meteorology*. 2d ed. John Wiley and Sons, 477 pp.

Kiemle, C., M. Kaestner, and G. Ehret, 1995: The convective boundary layer structure from lidar and radiosonde measurements during the EFEDA '91 campaign. *J. Atmos. Oceanic Technol.,* **12,** 771–782.

Kim, S.-W., S.-U. Park, and C.-H. Moeng, 2003: Entrainment processes in the convective boundary layer with varying wind shear. *Bound.-Layer Meteor.,* **108,** 221–245.

——, ——, D. Pino, J. V.-G. de Arellano, 2006: Parameterization of entrainment in a sheared convective boundary layer using a first-order jump model. *Bound.-Layer Meteor.,* **120,** 455–475.

Lenschow, D. H., 1970: Airplane measurements of planetary boundary layer structure. *J. Appl. Meteor.,* **9,** 874–884.

——, 1974: Model of the height variation of the turbulence kinetic energy budget in the unstable planetary boundary layer. *J. Atmos. Sci.,* **31,** 465–474.

Lewellen, D. C., and W. S. Lewellen, 1998: Large-eddy boundary layer entrainment. *J. Atmos. Sci.,* **55,** 2645–2665.

——, and ——, 2000: Boundary layer entrainment for different capping conditions. Preprints, *14th Symp. on Boundary Layers and Turbulence,* Aspen, CO, Amer. Meteor. Soc., 80–83.

Lilly, D. K., 1968: Models of cloud-topped mixed layers under a strong inversion. *Quart. J. Roy. Meteor. Soc.,* **94,** 292–309.

——, 2002a: Entrainment into mixed layers. Part I: Sharp-edged and smooth-edged tops. *J. Atmos. Sci.,* **59,** 3340–3352.

——, 2002b: Entrainment into mixed layers. Part II: A new closure. *J. Atmos. Sci.,* **59,** 3353–3361.

Mahrt, L., and D. H. Lenschow, 1976: Growth dynamics of the convectively mixed layer. *J. Atmos. Sci.,* **33,** 41–51.

Otte, M. J., and J. C. Wyngaard, 2001: Stably stratified interfacial-layer turbulence from large eddy simulation. *J. Atmos. Sci.,* **58,** 3424–3442.

Pino, D., J. V.-G. de Arellano, and P. J. Duynkerke, 2003: The contribution of shear to the evolution of a convective boundary layer. *J. Atmos. Sci.,* **60,** 1913–1926.

Press, W. H., S. A. Teukolsky, W. T. Vetterling, and B. P. Flannery, 1992: *Numerical Recipes in Fortran 77*. 2d ed. Cambridge University Press, 933 pp.

Sorbjan, Z., 1996a: Numerical study of penetrative and "solid lid" nonpenetrative convective boundary layers. *J. Atmos. Sci.,* **53,** 101–112.

——, 1996b: Effects cause by varying the strength of the capping inversion based on a large eddy simulation model of the shear-free convective boundary layer. *J. Atmos. Sci.,* **53,** 2015–2024.

——, 2004: Large-eddy simulation of the baroclinic mixed layer. *Bound.-Layer Meteor.,* **112,** 57–80.

Stull, R. B., 1973: Inversion rise model based on penetrative convection. *J. Atmos. Sci.,* **30,** 1092–1099.

——, 1976a: The energetics of entrainment across a density interface. *J. Atmos. Sci.,* **33,** 1260–1267.

——, 1976b: Internal gravity waves generated by penetrative convection. *J. Atmos. Sci.,* **33,** 1279–1286.

——, 1976c: Mixed-layer depth model based on turbulent energetics. *J. Atmos. Sci.,* **33,** 1268–1278.

——, 1988: *An Introduction to Boundary Layer Meteorology*. Kluwer Academic, 670 pp.

Sullivan, P., C.-H. Moeng, B. Stevens, D. H. Lenschow, and S. D. Mayor, 1998: Structure of the entrainment zone capping the convective atmospheric boundary layer. *J. Atmos. Sci.,* **55,** 3042–3064.

Tennekes, H., 1973: A model for the dynamics of the inversion above a convective boundary layer. *J. Atmos. Sci.,* **30,** 558–567.

——, and A. G. M. Driedonks, 1981: Basic entrainment equations for the atmospheric boundary layer. *Bound.-Layer Meteor.,* **20,** 515–531.

VanZanten, M. C., P. G. Duynkerke, and J. W. M. Cuijpers, 1999: Entrainment parameterization in convective boundary layers. *J. Atmos. Sci.,* **56,** 813–828.

Zeman, O., and H. Tennekes, 1977: Parameterization of the turbulent energy budget at the top of the daytime atmospheric boundary layer. *J. Atmos. Sci.,* **34,** 111–123.

Zilitinkevich, S. S., 1991: *Turbulent Penetrative Convection*. Avebury Technical, 179 pp.